AD-A138 930 A REVIEW STUDY OF NONDESTRUCTIVE TEST TECHNIQUES FOR RESIDUAL STRESSES IN..(U) DAYTON UNIV OH RESEARCH INST B B RAJU JAN 84 UDR-TR-83-70 AFWAL-TR-83-3108 1/1

UNCLASSIFIED F33615-80-C-3401 F/G 14/2 NL

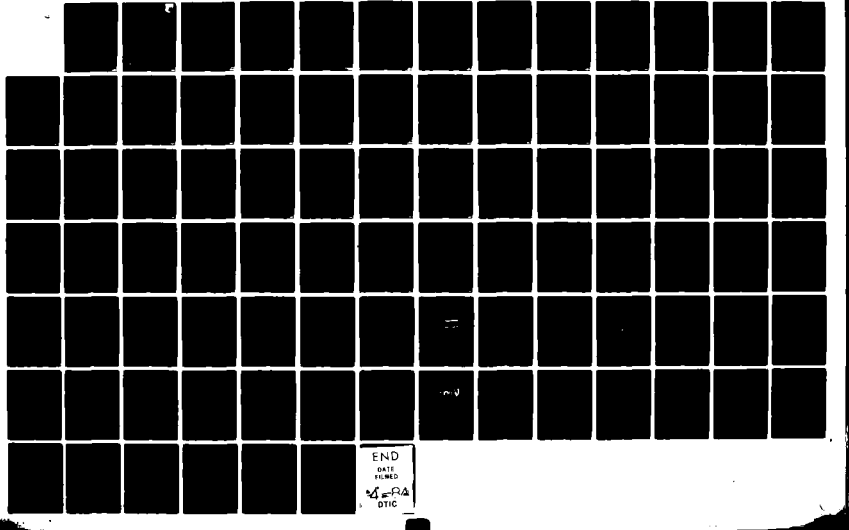

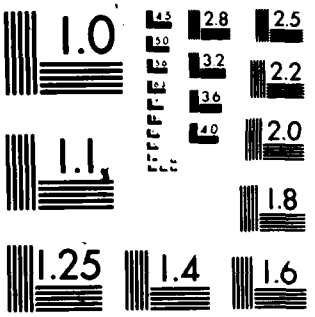

AFWAL-TR-83-3108

AD A138930

A REVIEW STUDY OF NONDESTRUCTIVE TEST TECHNIQUES FOR RESIDUAL STRESSES IN AIRCRAFT TRANSPARENCIES

B. Basava Raju
University of Dayton Research Institute
300 College Park Avenue
Dayton, Ohio 45469

January 1984

Final Report for Period June 1982 - December 1982

Approved for public release; distribution unlimited.

DTIC FILE COPY

FLIGHT DYNAMICS LABORATORY
AIR FORCE WRIGHT AERONAUTICAL LABORATORIES
AIR FORCE SYSTEMS COMMAND
WRIGHT-PATTERSON AIR FORCE BASE, OHIO 45433

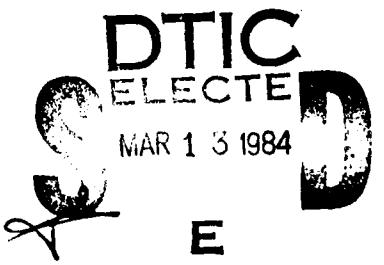

NOTICE

When Government drawings, specifications, or other data are used for any purpose other than in connection with a definitely related Government procurement operation, the United States Government thereby incurs no responsibility nor any obligation whatsoever; and the fact that the government may have formulated, furnished, or in any way supplied the said drawings, specifications, or other data, is not to be regarded by implication or otherwise as in any manner licensing the holder or any other person or corporation, or conveying any rights or permission to manufacture use, or sell any patented invention that may in any way be related thereto.

This report has been reviewed by the Office of Public Affairs (ASD/PA) and is releasable to the National Technical Information Service (NTIS). At NTIS, it will be available to the general public, including foreign nations.

This technical report has been reviewed and is approved for publication.

ROBERT J. SIMMONS, 1Lt, USAF
Project Manager
Advanced Development Branch
Vehicle Equipment Division

RALPH J. SPEELMAN
Program Manager
Advanced Development Branch
Vehicle Equipment Division

FOR THE COMMANDER

SOLOMON R. METRES
Director
Vehicle Equipment Division

"If your address has changed, if you wish to be removed from our mailing list, or if the addressee is no longer employed by your organization please notify AFWAL/FIEA, *W-PAFB, OH 45433 to help us maintain a current mailing list".*

Copies of this report should not be returned unless return is required by security considerations, contractual obligations, or notice on a specific document.

Unclassified

SECURITY CLASSIFICATION OF THIS PAGE (When Data Entered)

REPORT DOCUMENTATION PAGE		READ INSTRUCTIONS BEFORE COMPLETING FORM
1. REPORT NUMBER AFWAL-TR-83-3108	2. GOVT ACCESSION NO. AD-A138930	3. RECIPIENT'S CATALOG NUMBER
4. TITLE (and Subtitle) A REVIEW STUDY OF NONDESTRUCTIVE TEST TECHNIQUES FOR RESIDUAL STRESSES IN AIRCRAFT TRANSPARENCIES		5. TYPE OF REPORT & PERIOD COVERED Final Report June 1982 - Dec. 1982 6. PERFORMING ORG. REPORT NUMBER UDR-TR-83-79
7. AUTHOR(s) B. Basava Raju		8. CONTRACT OR GRANT NUMBER(s) F33615-80-C-3401
9. PERFORMING ORGANIZATION NAME AND ADDRESS University of Dayton Research Institute 300 College Park Avenue Dayton, OH 45469		10. PROGRAM ELEMENT, PROJECT, TASK AREA & WORK UNIT NUMBERS Program Ele. 64212F Project 1926 Task 192601 WU#19260104
11. CONTROLLING OFFICE NAME AND ADDRESS Air Force Wright Aeronautical Laboratories (AFWAL/FIEA) Wright-Patterson AFB, OH 45433		12. REPORT DATE January 1984 13. NUMBER OF PAGES
14. MONITORING AGENCY NAME & ADDRESS(if different from Controlling Office)		15. SECURITY CLASS. (of this report) Unclassified 15a. DECLASSIFICATION/DOWNGRADING SCHEDULE

16. DISTRIBUTION STATEMENT (of this Report)

Approved for public release; distribution unlimited.

17. DISTRIBUTION STATEMENT (of the abstract entered in Block 20, if different from Report)

18. SUPPLEMENTARY NOTES

19. KEY WORDS (Continue on reverse side if necessary and identify by block number)

Residual stress
Crazing
Aircraft transparencies
Scattered-light photoelasticity
Ultrasonics
Rayleigh surface waves
Magneto-photoelasticity
Laser diffraction

20. ABSTRACT (Continue on reverse side if necessary and identify by block number)

The main objectives of this program are to (1) conduct review studies on candidate nondestructive test techniques for determining residual stresses in aircraft transparencies; (2) identify and recommend nondestructive test techniques having potential for further laboratory development and field use. The program consisted of three primary tasks: (1) a comprehensive general literature review of over 150 publications on holography, x-rays, moiré, scattered-light, thermal methods, ultrasonic techniques, acoustic →

DD FORM 1 JAN 73 1473 EDITION OF 1 NOV 65 IS OBSOLETE

Unclassified

SECURITY CLASSIFICATION OF THIS PAGE (When Data Entered)

Continuation of Block 20.

emission, magneto-photoelasticity, integrated photoelasticity, laser diffraction, and eddy current technique; (2) a detailed literature review on scattered light photoelasticity, ultrasonic technique I based on the Rayleigh surface waves, ultrasonic technique II based on the ultrasonic energy reflection at a liquid-solid interface magneto-photoelasticity, and laser diffraction; (3) detailed review studies on scattered-light techniques and ultrasonic techniques I and II.

The studies revealed that the basic principles and experimental procedure of ultrasonic technique I based on Rayleigh surface waves is fairly well developed. The experimental hardware is simple, cheap, commercially available, and can readily be employed for field measurements. The scattered-light technique is one of the well developed methods available to a stress analyst. Besides residual stresses, it has other capabilities such as dynamic, static, thermal, and elasto-plastic stress determination. Very sophisticated experimental hardware is commercially available. At present this technique is more suitable as a laboratory tool as it needs the expertise of a well trained engineer; however, the possibilities of its use in the field environment exist. Ultrasonic technique II, based on energy reflection at a liquid-solid interface, magneto-photoelasticity, and laser diffraction all need further development.

It is recommended that: (1) ultrasonic technique I, based on Rayleigh surface waves, be evaluated for use on aircraft transparency plastic materials such as polycarbonates and acrylics and be further considered for development as a field tool to nondestructively determine the residual stresses in aircraft transparencies in their installed condition; (2) scattered-light techniques be demonstrated as a nondestructive technique for quantifying residual stresses in aircraft transparencies in the laboratory and that the experimental hardware required for field use be defined and, if practical, developed.

FOREWORD

The effort reported herein was conducted for the Air Force Wright Aeronautical Laboratories, Flight Dynamics Laboratory, Wright-Patterson Air Force Base, Ohio, under Contract F33615-80-C-3401/P00007, Project 1926. Air Force administrative direction and technical support was provided by Lt. Robert Simmons. The work described herein was conducted during the period June 1982 through December 1982. Project supervision was provided by Mr. Dale H. Whitford, Supervisor, Aerospace Mechanics Division, University of Dayton Research Institute. Technical direction was provided by Mr. Blaine S. West, head, Applied Mechanics Group.

The author wishes to acknowledge the untiring efforts of Mrs. Judith N. Hecht for procuring over 150 publications which formed the basis of this review study.

TABLE OF CONTENTS

TABLE OF CONTENTS

LIST OF ILLUSTRATIONS

LIST OF SYMBOLS

A	Maximum amplitude of plane polarized light
a	Distance to outer surface of four-point bending specimen from neutral axis
A_1	Vibrational displacement of linearly polarized light
A_2, A_3	Vibrational displacement of circularly polarized light
A_4, A_5	Vibrational displacement components of light resolved along the directions of the secondary principal axes
A_6, A_7	Vibrational displacement component of light normal to the directions of observation OA and OB, respectively
A, B	Arbitrary constants used in the expressions for ϕ and ψ
a, b	Distance from pivot A and radius of roller B in the goniometer
A, B	Pivot points in the goniometer
$\bar{A}_6, \bar{A}_7$	Maximum amplitude of the light components A_6, A_7
A_R, A_i	Amplitude ratios of reflected and incident acoustic waves
A^*, B^*	Constants used in the energy ratios of acoustic waves
C	Compensator
c	Material stress-fringe constant
D	Reference point in the goniometer
d	Distance of the receiver from the reference point D

E, E_i	Strain tensor, principal values of strain tensor
f	Frequency of an acoustic wave in a material
H	Height to the reference point D of the goniometer
h_1, h_2	Heights to pivot points $\tilde{A}$ and $\tilde{B}$, respectively, of the goniometer
K	Wave number
K_ℓ, K_t	Wave number for the longitudinal and shear waves
K_S	Constant which depends upon the light scattering property of the material
K_O	Bulk modulus
K_B	A proportionality constant used with the bending stress at any location in the thickness of a beam
L_1/L_2	Lens system to choose a pencil operation of light
$L_4/L_5/L_6/L_7$	Lens system to choose the ribbon operation of light
L_8, L_9	Lenses
ℓ, m, n	Murnaghan third-order elastic constants for an isotropic material
ℓ_1, m_1, n_1	Direction cosines of an outer normal to a surface
N	Coordinate in the normal direction
ON	Normal direction in a model
$\bar{N}$	Photoelastic fringe order
ON'	Direction making an angle θ with ON

N', N''	Coordinates in the ON'-direction
O, O_1	Origin of coordinate system
P	Pivot point for the goniometer
$p', q'; p'', q''; p''', q'''$	Secondary principal stresses in xy-, xz-, and yz-planes in XYZ coordinate system
$p^*, q^*; p^{**}, q^{**}$	Secondary principal stresses in Xy- and Ty-planes in XYN and YTN' coordinate systems
p_o	Magnitude of hydrostatic stress
p_1, p_2	Uniaxial stresses indirections 1 an 2
R, L, S, I	Energies of reflected, longitudinal shear, and incident acoustic waves in a li 'solid interface
q, s	$\sqrt{k^2-k_l^2}$, $\sqrt{k^2-k_t^2}$ derived wave numbers
T	Uniaxial tension
t	Time
t_s, t_{so}	Transit time for stressed and unstressed specimen
U, V	Ratios of intensity of scattered light observed while the model is under load to that observed while it is free of load along the directions OA and OB, respectively
U_R, W_R	Rayleigh wave displacements in the x- and z-directions
$\vec{v}$	Particle displacement vector in a material medium
V_{RO}, V_{SO}	Raleigh wave velocity and shear wave velocity for a stress-free isotropic medium
V_R, V_S	Rayleigh wave velocity and shear wave velocity in a stressed medium

V_{Sy}, V_{Sz}	Velocities of shear waves polarized in Y and Z directions
V_{12}, V_{13}	Velocities of shear waves propagating along the 1-direction and polarized along the 2- and 3-directions, respectively
V_{L1}, V_{L2}, V_{S2}	Longitudinal wave velocity in water (medium-1), longitudinal and shear wave velocities in the material (medium-2)
S_x, S_{max}, S_{ave}	Bending stress at a distance x from the outer surface, maximum bending stress and average bending stress
x,y,z	Cartesian coordinate system
α	Angle between the secondary principal axes in the model and the axes of the quarter-wave plate
C_5, C_6	Second-order elasticity constants (Truesdell)
$\lambda_i, \lambda_1, \lambda_2, \lambda_3$	Principal extensions (Bach and Askegard)
δ	Relative displacement components of light after it emerges from the model
δ_6, δ_7	Phase angles of light components A_6 and A_7
ψ', ψ'', ψ'''	Orientations of p', p", and p"' secondary principal stress components with respect to x, y, and z axes, respectly
ψ^*, ψ^{**}	Orientations of p* and p** secondary principal stress compcnents with respect to x and T axes, respectively
ϕ, χ	Potential functions defining the longitudinal and shear waves
	Poisson's ratio
ω	Angular velocity of a polarized light or circular frequency of acoustic wave motion in solids

ρ_o, ρ	Mass density in the undeformed and deformed state, respectively
ρ_1, ρ_2	Densities of liquid and solid in a liquid/solid interface
λ, μ	Second-order Lamé constants for an isotropic material
λ_R	Rayleigh wave length
λ_M	Wave length of an acoustic wave in a material
$\sigma_x, \sigma_y, \sigma_z$	Normal-stress components in Cartesian coordinates X, Y, and Z
σ_{xx}, σ_{zz}	Rayleigh wave normal-stress components in Cartesian coordinates X, Y, and Z
σ_{XZ}	Rayleigh wave shear-stress component in Cartesian coordinate x, y, and z
$\sigma_{xx/x=0}$	Rayleigh wave normal-stress component on the surface
$\sigma_1, \sigma_2, \sigma_3$	Principal stresses
$\tau_{xy}, \tau_{xz}, \tau_{yz}$	Shear-stress components in Cartesian coordinates X, Y, and Z
σ_N, τ_{YN}	Normal- and shear-stress components in Cartesian coordinates X, Y, and N
θ	Angular coordinate
$\alpha_1, \alpha_2, \alpha_3$	Principal stretches (Bach and Askegaard)
$\theta_i, \theta_l, \theta_s$	Incident angle, refraction angles of longitudinal and shear waves in a liquid/solid interface
θ_1, θ_2	Critical angles at a liquid/solid interface
W_R	Rayleigh wave normal displacement amplitude
W_{OR}	Rayleigh wave normal displacement amplitude on the surface
1,2,3	Acoustic axes in a solid

SECTION 1
INTRODUCTION

1.1 PROGRAM OBJECTIVES AND SUMMARY

Experience has shown that surface crazing and delamination of a laminated plastic transparency are related to the residual stress levels in the transparency. It has been theorized that control of this stress level (during the manufacturing and installation process) to a critical threshold value may increase the transparency's service life by delaying the need to remove them due to either of these stress induced failures.

The main objectives of this program are to (1) conduct review studies on candidate nondestructive test techniques for determining residual stresses in aircraft transparencies; (2) identify and recommend nondestructive test techniques having potential for further laboratory development and field use.

The program was organized under three primary tasks: (1) a comprehensive general literature review of over 150 publications on holography, x-rays, moiré, scattered-light, thermal methods, ultrasonic techniques, acoustic emission, magneto-photoelasticity, laser diffraction, and eddy currents; (2) a detailed literature review on scattered-light photoelasticity, ultrasonic technique I based on the Rayleigh surface waves; ultrasonic technique II based on the reflection of ultrasonic energy at a liquid-solid interface, magneto-photoelasticity, and laser diffraction; (3) detailed review studies on scattered-light techniques and ultrasonic techniques I and II.

The detailed studies on scattered-light techniques included the principles of the dual-observation method; the scattered-light photoelastic properties of aircraft transparency plastics; the scattered-light photoelastic device; and the procedures to determine the residual stresses at the surface and through the thickness.

The detailed studies on ultrasonic technique I included the concept of Rayleigh waves (their structure and properties); the

propagation of Rayleigh waves in a stressed elastic medium; the stress-velocity expressions for uniaxial and general stress fields; the ultrasonic stress measuring device; and the procedures to determine the residual stresses at the surface and through the thickness.

The detailed studies on ultrasonic technique II based on the reflection of energy at a liquid-solid boundary included the basic principles and the equations; and the principles, calibration, and application of a goniometer for the residual stress determination.

These methods were compared and evaluated as to their potential use in the laboratory and/or field for the determination of the residual stresses in aircraft transparencies, and recommendations have been made.

1.2 BACKGROUND INFORMATION

1.2.1 Residual Stress

Internal or residual stresses have been defined as those existing in bodies upon which no external forces are acting. They can arise out of unequal plastic deformation, causing a misfit of the elements upon removal of the load; alternately, a chemical change may alter a part of the body and similarly produce residual stresses. Residual stresses fall naturally into two categories. First, external forces can influence differently various parts of a body, and thus, even though the material may be isotropic and homogeneous, residual stresses may be produced. Secondly, textural inhomogeneities of the material may give rise to internal stresses from external influences which are acting uniformly upon the body. The residual stresses of the first group, arising, for example, out of a deformation or forming process, are often large and well defined in their distribution. They are called macrostress. The other group contains residual stresses (caused, for example, by quenching a two-phase alloy) which are usually on a granular scale and often randomly distributed. These are termed microstress, or residual stresses of the second

kind. The microstress are, in general, uniformly tensile or compressive in a particular grain, but tentative suggestions of a subgranular variation have been made and have led to the idea of microstress of a third kind.

1.2.2 Stress Crazing

All of the transparent plastic materials currently available are susceptible to crazing, though in widely varying degrees. Crazing has been defined as fine cracks which may extend in a network over or under the surface or through a plastic. These fine cracks are often difficult to discern, because they are approximately perpendicular to the surface, very narrow in width, and usually not over 0.001 inch in depth. They can be seen by reflection from their surfaces and appear as bright lines when the specimen is viewed at varying angles to the incident light (References 1 to 4).

Crazing results from a variety of causes, the more prominent of which are: (1) residual stresses caused by uneven stretching and cooling involved in forming; (2) contact with solvents and solvent vapors in the manufacture, operation, and servicing of aircraft, including the adhesives used in making joints; and (3) stresses induced in the material by machining, polishing, mounting, and other fabrication and flight operations. When the craze cracks are in a random pattern, the crazing can usually be ascribed to the action of solvent vapors and is referred to as solvent crazing. When the cracks are approximately parallel, the crazing is usually due to the application of mechanical stresses and is referred to as stress crazing. These two types are not mutually exclusive, so that the effect may be produced by the simultaneous action of stress and solvent, referred to as stress-solvent crazing. Internal stress is, in fact, essential to solvent crazing. In stress crazing and stress-solvent crazing, the craze cracks appear perpendicular to the tensile component of the applied stress. Tensile and flexural stresses cause crazing, whereas purely compressive stresses do not produce crazing.

Crazing reduces the luminous transmittance of the transparent plastic materials and interferes with vision, especially when the aircraft is flying into the sun. It also affects the structural properties of the plastics. Crazing cracks 0.006 inch deep resulted in a 30 percent loss in tensile strength of a plastic material in one investigation (Reference 1). The extreme stress concentration at the base of a fissure results in propagation of the crazing with time under load. Small changes in crack depth are accompanied by large decreases in the impact strength. In extreme cases crazing can reduce tensile, flexural, and impact strengths to virtually zero.

Long-time cantilever loading of test specimens (FTMS 406 Method 6053) with and without various solvents applied to the tensile surface has been used to estimate the threshold crazing stress under various conditions.

In References 2 and 3, the phenomena associated with the crazing of cast polymethyl methacrylate sheet are described and examined in the light of earlier work. The theory is advanced that ordinary elastic stresses produced in the surface during polymerization cause local rupture under the plasticizing influence of absorbed solvent or when sufficiently increased by an externally applied stress. The heat treatment of the sheet to minimize crazing and to produce material free from distortion is described. In Reference 4, crazing effects are described in polystyrene; evidence of crazing is noted at various points on the specimen where stress concentration occurs, such as at regions where the specimen changes its cross-sectional dimensions or at points of concentrated load application.

1.2.3 A Review Study of Literature on the Analysis and Methods of Nondestructive Test Techniques to Determine the Residual Stresses

The following paragraphs describe nondestructive test techniques used to determine residual stresses.

1.2.3.1 Scattered-Light Photoelasticity

Some of the earlier work on scattered-light photoelasticity was performed by Weller (References 5 and 6) in

the United States, and by Jessop (Reference 7) in the United Kingdom, but a systematic study of the analysis and experiments on scattered-light photoelasticity was initiated by Frocht and Srinath (References 8, 9, 10, and 11). In Reference 8, the basic theory of scattered light is developed and experimental evidence provided shows the accuracy possible in the determination of the isoclinic parameters and birefringence. The possibilities of the method are further demonstrated by determining the stress distribution along critical lines in a diametrically compressed sphere and comparing the results with theory and previous experiments. Srinath (Reference 10) discusses the inaccuracies in the various exact methods to determine the difference of the secondary principal stresses and their directions at any general point. Further, he proposes a new method called the mini-max method to improve the accuracy.

Cheng (References 12, 13, 14, and 15) describes various techniques for determining the directions of the secondary principal stresses and their difference in scattered-light photoelasticity, without using a compensator but still capable of obtaining the same degree of accuracy. In Reference 13, a dual-observation method is developed for determining the photoelastic parameters in scattered light. Using this method, the intensities of scattered light along two directions of observation, making an angle of 45 degrees in a plane normal to the beam, are recorded simultaneously without rotation of either the light beam or the model. Photoelastic parameters are evaluated from these records. The theory of the method, the apparatus and procedures, as well as an illustrative experiment, are reported. In Reference 14, Cheng describes a development of an automatic data-collecting-and-interpreting system for a dual-observation method in scattered-light photoelasticity. The system incorporates a flexible relay optic, photon counting, and computer techniques. Photoelastic parameters are evaluated from the photon counts by means of an electronic digital computer. Evaluation procedures have been improved so that the effect of absorption of scattered light is eliminated, and the rotation of the secondary principal axes is considered. Experiments were performed for cases with stationary as well as rotating

secondary principal axes. In Reference 15, Cheng reports the experiments conducted on an aircraft windshield sample having a three-layer (glass-vinyl-glass) sandwich structure. Photographs of fringe patterns in scattered light are shown, and the stress distribution across the thickness of glass layer is determined. Bateson, et al., reports residual stress measurements in tempered glass plates by scattered light method with a laser source in Reference 16.

Swinson applies the scattered light methods to transient thermal stress problems in a solid propellant rocket motor and develops a theory and technique for locating critical stress points in a structural component which can be utilized to reshape the structural components surface to minimize stress in critical regions (References 17, 18, 19, and 20). Scattered-light technique has a tremendous potential for three-dimensional dynamic stress analysis problems (Reference 21). Reference 22 describes a scattered-light rosette to determine the state of stress on a free surface. Three simultaneously polarized light beams intersecting at a surface point yield sufficient scattered-light photoelastic data to evaluate the stresses at a surface point. After initial calibration, the surface stress analysis consists of recording a series of photographs, one photograph for each point of interest. General equations are derived which are valid for any three light beams intersecting at a surface point on a stressed photoelastic material. Stresses obtained from the scattered-light rosette analysis are compared with the known solutions for two problems. Reference 23 reports the use of scattered-light photoelasticity to solve doubly connected tapered-shaft problems. Some techniques are presented which help realize more fully the potential of scattered-light photoelasticity. These include the use of a continuous-emission gas laser as a light source for the polariscope, the use of a photometer arrangement to read fringe spacings, and the use of curve-fitting techniques to analyze the data. Also, some design features for constructing a scattered-light polariscope are presented.

In Reference 24, a set of equations is presented and the effect of rotation of the secondary principal stress axes is described. The equations, general and relatively simple, adequately describe observed results. In studying the equations, a better understanding of the rotational effect can be achieved, and a technique is suggested which can eliminate any error resulting from rotation. This technique and the concepts involved are substantiated with experimental evidence.

Sutliff investigates three-dimensional stresses in models of composite materials with discontinuous fibers using the scattered-light photoelastic method (Reference 25). The scattered-light method is applied to plane-stress problems in Reference 26. The results show that one full-field photograph is sufficient to determine the state of stress in the model as well as to calibrate the model material. Results for the case of a ring in diametral compression are presented.

Johnson has employed the scattered-light technique to determine the stresses and strains in a shaft with a circumferential groove subjected to torsion loading beyond the elastic limit (References 27 and 28). Gross-Peterson (Reference 29) investigates the birefringence and, thereby the stresses in a photoelastic model utilizing the light scattered from a beam of light propagating through the model. The retardance from the entry point of the light beam into the model to a certain point along the beam is expressed in terms of the intensity of the scattered light. The retardance for a short distance along the light path within the model is determined as a function of the total retardances from the entry point of the model to the two end points of the distance investigated.

The lack of understanding of the effect of the rotation of secondary principal axes has been a severe limitation of the scattered-light method. In Reference 30, Cernosek applies the method of Poincare's equivalent system in order to

develop a general formula for scattered-light intensity. Relationships among the orientation of eigenvectors and their phase retardation and stresses have been found. The method is illustrated by the solution of the problem of a circular rod loaded by a combination of torsion and axial load. An experimental procedure has also been suggested. Robert (References 31 and 32) applies the principle of polarization of scattered light to determine the principal stresses in the interior of a model. On the basis of the theorem which states that "a series of birefringents is equivalent to a unique birefringent, followed by a medium endowed with rotational power," it can be assumed that, if the characteristics of a series of birefringents are known, it is possible to find the characteristics of an interior section.

Reference 33 reports the results of an investigation and extension of the various proposed procedures and methods of analysis for the photoelastic determination of three-dimensional state of stress. Two important limitations of the previous developments are removed. The rotation of the axes of the secondary principal stress in the planes perpendicular to the path of the light wave is to be considered at every point along the path of the light wave traveling in a stressed three-dimensional medium. Also, methods for the analysis of whole planes are presented, thus avoiding the cumbersome and tedious point-by-point procedures that have been advanced.

Berghaus (Reference 34) presents a method for obtaining scattered light photoelastic data in three-dimensional problems using an unpolarized incident light beam. Using simplifying optical assumptions, the scattered-light observation path is considered to be a series of half-wave retarders. Data are obtained through rotation of the optical analyzer and translation of the incident light beam with respect to the model. The method is applied to obtain data in problems where the secondary principal directions are (1) fixed and (2) rotate. Results compare favorably with those obtained using a polarized incident beam.

Stresses and strains in axisymmetric problems are found by using scattered-light photoelasticity (Reference 35). Three retardation measurements and the strain-displacement relations in cylindrical coordinates are used to find the complete state of stress and strain. The method is demonstrated on a static shrink-fit problem.

In References 36 and 37, a scattered light polariscope and its principle of operation are described.

1.2.3.2 The Ultrasonic Technique I: Using Rayleigh Waves

Reference 38 describes a technique which utilizes ultrasonic radiation to measure residual stresses in metals. This technique makes it possible to detect and measure the magnitude of the principal stresses and also to obtain their direction. The velocities of ultrasonic waves in materials are measured as the time to travel a fixed path length, and the change in transit time is related to the applied stress. The linear relationship obtained allows a procedure based on this principle to be used for the measurement of residual stress using surface waves and shear waves. A method for plotting stress profiles through a material using surface waves uses varying frequencies for the ultrasonic wave. The system used for this technique is called the "Modified Time of Flight System." In Reference 39, an ultrasonic shear wave technique to measure stress in metals is described. The technique utilizes a pulse-echo system operating at 7 MHz to measure changes in the time of travel of the ultrasonic shear wave. Linear changes in the velocity of a shear wave occur with stress and are dependent on the higher order elastic constants of the material. Measurements using the ultrasonic technique of simulated residual stress, introduced by bending of a 6-foot section of steel I-beam, yielded values in the vicinity of those measured using strain gages.

Martin (Reference 40) evaluated the feasibility of using an ultrasonic nondestructive technique for measuring applied and residual stresses in metals; specifically,

surface and near-surface stresses in aluminum alloys. In Reference 41, he describes an investigation of the relative effects of uniaxial stress and preferred grain orientation on the Rayleigh wave velocity in aluminum. The calculation of the relationship between Rayleigh wave velocity and stress is based on second order elasticity theory. He postulates a linear relationship between velocity and grain orientation. He concludes that changes in velocity due to uniaxial stress in the elastic range and preferred grain orientation are of the same order of magnitude. He reviews some experimental data and compares it with theoretical calculations. Gordon and Speidel (Reference 42) describe ultrasonic instrumentation and transducers utilized for several types of stress measurements in commercial alloys such as aluminum and low carbon steel. Comparison with other experimental methods such as strain gages and x-ray diffraction are also discussed. The instrumentation was designed to measure the time of flight of a propagated ultrasonic wave with a resolution of 0.2 nanoseconds.

Reference 43 reports studies of local variations of Rayleigh (surface) circumferential ultrasonic wave velocity near a pipe-girth welded in large-diameter thin-wall type stainless steel pipe. The residual stress distribution was estimated independently from shell theory for an elastic, infinite, thin shell with circumferential line load. The pattern of surface wave velocity variation matched the theoretical residual stress pattern closely.

McKannan (Reference 44) calibrates and evaluates ultrasonic methods by conducting tests on a beam subjected to bending loads. The frequency employed has seven megacycles per second which provided a depth of penetration of one millimeter. The measurement accuracy of the time of flight was 0.1 nanosecond (or 10^{-8} seconds) and the resolution or sensitivity of the ultrasonic method was less than 100 psi in 2024-T3 aluminum alloy.

Reference 45 describes an ultrasonic stress analyzer and surface stress and bulk stress tranducers.

1.3.3. Ultrasonic Velocity-Stress Relations and Third Order Elastic Constants

In References 46 to 49, expressions for the velocities of elastic waves in stressed solids are derived using Murnaghan's theory of finite deformations and third-order terms in the energy. For isotropic materials, in addition to the Lamé constants λ and μ three additional constants, l, m, and n are required to describe the material. By measuring the transmission time of elastic pulses through the material, the velocities of longitudinal and shear waves are determined as a function of applied stress. By subjecting the material to hydrostatic pressure as well as simple compression, it is found that seven functions of the three constants l, m, and n can be measured and thus numerical values calculated. Results are given for polystyrene, iron, and Pyrex glass.

Cook and Valkenburg (Reference 50) review the theory of mechanical wave propagation along the surface of an extended solid medium, adapting it to nondestructive materials testing. Lockett (Reference 51) describes the propagation of Rayleigh waves in an isotropic thermoelastic solid. It is found that taking into account the thermal properties of the solid produces a difference of less than one percent in the velocity and amplitude of the Rayleigh waves.

McSkimin (References 52 and 53) describes the aspects of wave propagation of particular importance for the measurement of elastic moduli of solids. Measurements have been made for all six third-order elastic moduli of germanium by measuring ultrasonic velocities in selected directions when directed static stresses are applied to the crystal. Using the finite strain formulas of Murnaghan, the measured velocities are related to the three second-order elastic moduli and the six third-order elastic moduli.

Toupin and Bernstein (Reference 54) derive the general equations for a small displacement superimposed on a finite deformation of a perfectly elastic material of arbitrary

symmetry. It is shown that the variation of sound speeds with initial stress and the measured magnitude of the acoustoelastic effect can be used to determine the third-order elastic constants of an isotropic material and as a partial confirmation and experimental check of the theory.

Bradfield (References 55 and 56) enumerates methods of using vibrations to determine the values of elastic constants which are most promising and offers advice to show which method is best to use in a given set of circumstances. The methods described are also applicable to non-metals especially those of hard, crystalline, glass-like, or ceramic natures.

Thurston (References 57 and 58) derives exact expressions for the sound velocity and for a natural velocity and their stress derivatives, evaluated at zero stress, in terms of second- and third-order elastic constants.

Smith, et al. (Reference 59) have determined the third-order elastic moduli of several isotropic polycrystalline metals from measurements of the velocities of both longitudinal and shear ultrasonic waves in uniaxially stressed specimens. In each case, the wave-propagation direction was chosen normal to the applied stress, and the shear waves were polarized either normal or parallel to the stress direction. Hence, a unique evaluation of all three third-order moduli was possible, using the theory of Thurston and Brugger, specialized for isotropic symmetry. The measuring equipment is based on a new variation of the pulse-echo interferometric technique and is capable of resolving velocity changes of a few parts in 10^6. Results are presented for several steels, aluminum alloys, magnesium, tungsten, and molybdenum, and are shown to be in good agreement with alternative nonlinear elastic data, including static measurement of the pressure derivatives of the bulk and shear moduli.

The concept of Rayleigh waves, their structure and properties, are discussed in Reference 60. Propagation of Rayleigh waves on cylindrical and spherical surfaces as well as at an interface with a liquid are discussed. In

Reference 61, the wave propagation [illegible] investigated theoretically by Thurston's method in the homogeneously stressed crystals with any symmetry and formulate the acoustical birefringent relations. The theoretical and experimental [illegible] Rayleigh surface waves are discussed in [illegible].

[illegible] have derived expressions for the [illegible] of transverse waves in a body with an arbitrary stress field on the basis of a general theory formulated by Truesdell. These expressions for uniaxial and triaxial stress fields [illegible] difference in the principal stresses normal to the direction of wave propagation and the relative difference in velocity between two transverse waves that both propagate along one principal stress direction and that are polarized along the other two. Tests carried out with a uniaxial stress field have confirmed the existence of proportionality.

Okada (Reference 64) proposed new equations for stress measurement in orthotropic materials by ultrasonic birefringence techniques. Intensity of stress-induced anisotropy and its principal direction are related to the applied stress through three coefficients, in contrast to only one coefficient required for isotropic materials. Experiments of ultrasonic birefringence were carried out to determine the three coefficients in a plate of aluminum alloy with a slight orthotropy originated from roll working. Anisotropy induced by uniaxial stress and rotation of the principal axis were observed in several specimens with different directions of rolling. The results are in good agreement with the curves theoretically predicted by the equations proposed, showing the validity and usefulness of these equations for stress measurements in conventional materials.

In Reference 65, the basic relations of the acoustoelasticity are deduced by means of the infintesimal wave propagation in a deformed isotropic elastic material.

1.2.3.4 Ultrasonic Technique II: Reflection of Ultrasonic Energy at a Liquid-Solid Interface

Reference 66 reports the principles and construction of an ultrasonic goniometer for surface stress measurement in steel. The goniometer methods are potentially more useful where it is desired to obtain indications of the stresses, particularly residual stress, rather than loading stress (although both can be measured) at or near the surface of an object. The variation of the energy reflected from an interface as a function of angle of incidence and reflection (equal) using a suitably constructed goniometer should reveal marked changes in the vicinity of critical angles, and when a Rayleigh surface wave is generated in a solid with incident beam in a liquid. In Reference 67, Mayer reports the energy ratios of reflected and refracted waves to the incident wave at the liquid-solid boundaries as a function of the angle of incidence. The influence of the wave velocities in the media and media density on the shape of the curves is discussed. Ergin (Reference 68) reports the energy ratios of seismic waves reflected and refracted at a discontinuity. Rollins (References 69 and 70) establishes that the ultrasonic reflectivity of a liquid-solid interface can be a sensitive indicator of near-surface properties of the solid. At angles of incidence slightly less than that which produces total reflection, the reflectivity often falls off sharply with a minimum occurring at some angle $\overline{\theta}_2$. The value of $\overline{\theta}_2$ and the reflectivity at $\overline{\theta}_2$ are both frequency-dependent. It is often possible to find a frequency, f, which causes the reflectivity to approach zero at the minimum. Under these conditions, it is found that f, $\overline{\theta}_2$, and the reflection amplitude are all extremely sensitive to slight variations in such surface properties as elastic moduli, grain orientation or texture, attenuation, and degree of cold work. Further, it is reported that this technique can be used to detect changes in the properties of thin coatings or cladding on thicker substrates. Simplicity and ease of application

combined with inherent sensitivity make the technique a potentially powerful tool in nondestructive testing and material evaluation.

Bradfield (Reference 71) reports that the velocity of an ultrasonic surface wave is directly related to the elasticity of the material and hence to the stress residing in the surface layer. The goniometer measures this velocity over very small areas. Such measurements can be related to the texture and homogeneity of the material; they can help in ultrasonic hardness testing and they may be a means of detecting fatigue before failure.

Weinstein (Reference 72) reports on the failure of plane wave theory to predict the reflection of a narrow ultrasonic beam. In past studies of the interaction of an ultrasonic beam with a solid plate immersed in water, the general practice has been to assume that a narrow radiation pattern is a sufficiently close approximation to a plane wave to permit the use of plane wave theory to predict the results. Reflection measurements made in water with a three-degree radiation pattern at a frequency of 3.35 megacycles per second, using both air-backed aluminum plates of thickness ranging from 0.250 to 0.025 inch and a two-inch aluminum slab to approximate a semi-infinite medium, indicate that under certain conditions this assumption is not valid. Experimentally, the excess pressure of the reflected wave is considerably lower than that predicted by plane wave theory when the angle of incidence is such that the change of phase of the wave upon reflection varies greatly with a small change of the angle of incidence. It is apparent that at these angles of incidence a divergent beam which is several degrees wide cannot be used to approximate a plane wave. The nature of the phenomenon indicates that it should be of equal importance in the study of transmission phenomena.

1.2.3.5 Magneto-Photoelasticity

Aben (Reference 73) discusses the principles of magneto-photoelasticy and its applications. If a photoelastic model is placed in a magnetic field, the light vector

will rotate owing to the Faraday effect. An integral optical effect can therefore be observed with states of stress which do not show any optical effect by direct observation; for example, bending and quenching stresses in plates. Basic equations of magneto-photoelasticity are derived. An algorithm is developed which enables the optical phenomena to be determined in cases of arbitrary stress distribution along the wave normal. An investigation of bent plates is considered; a nomogram was produced which enables the stress components to be determined on the basis of experimental data. The experimental technique is described.

1.2.3.6 Laser Diffraction

The complex nature of fracture strength as affected by crazing of a glassy amorphous polymer is well recognized. Processes leading to the formation and growth of a system of crazes and subsequent nucleation and propagation of cracks must be fully understood before a satisfactory theory of fracture can be obtained. Among a large number of influencing factors, the inception and distribution of crazing plays a major role in analyzing the statistical strength behavior of a polymer exposed to stress. Reference 74 reports preliminary attempts to observe crazing through the application of laser diffraction techniques. It is reported that laser diffraction is extremely sensitive to the occurrence of crazing. Qualitatively, the diffraction patterns characterize faithfully the distribution of the crazes together with other features. Several light micrographs and corresponding laser diffraction patterns are illustrated in this reference. Quantitative data on the kinetics of the accumulation of crazing development was to be collected as a continuation of this research. However, nothing was found in the course of the literature search.

SECTION 2
SCATTERED-LIGHT PHOTOELASTIC TECHNIQUE

2.1 PRINCIPLES OF SCATTERED-LIGHT PHOTOELASTICITY: (DUAL-OBSERVATION METHOD)

A dual-observation method will be described for determining the scattered-light, photoelastic parameters (Reference 13). Using this method, the intensities of scattered light along two directions of observation, making an angle of 45° in a plane normal to the light beam, are recorded simultaneously without rotation of either the light beam or the model. Photoelastic parameters are evaluated from these records.

In establishing the relations between the intensity of scattered light and the photoelastic parameters, there are two cases to be considered. The first is that in which the secondary principal axes remain constant, while in the second case they rotate inside the stressed elastic medium.

Case 1: Secondary Principal Axes Remain Constant

Let the vibrational displacement of a beam of linearly polarized light be given by

$$A_1 = A \sin\omega t \tag{1}$$

where A is the amplitude of the vibration, ω its angular velocity, and t the time (Figure 1). After passing through a quarter-wave plate, whose axes makes angles of $\pi/4$ radians with the plane of polarization of the incident beam, the emerging beam is circularly polarized and may be represented by two components along the axes. Thus,

$$A_2 = (2)^{-1/2} A \sin\omega t \tag{2}$$

and

$$A_3 = (2)^{-1/2} A \cos\omega t \tag{3}$$

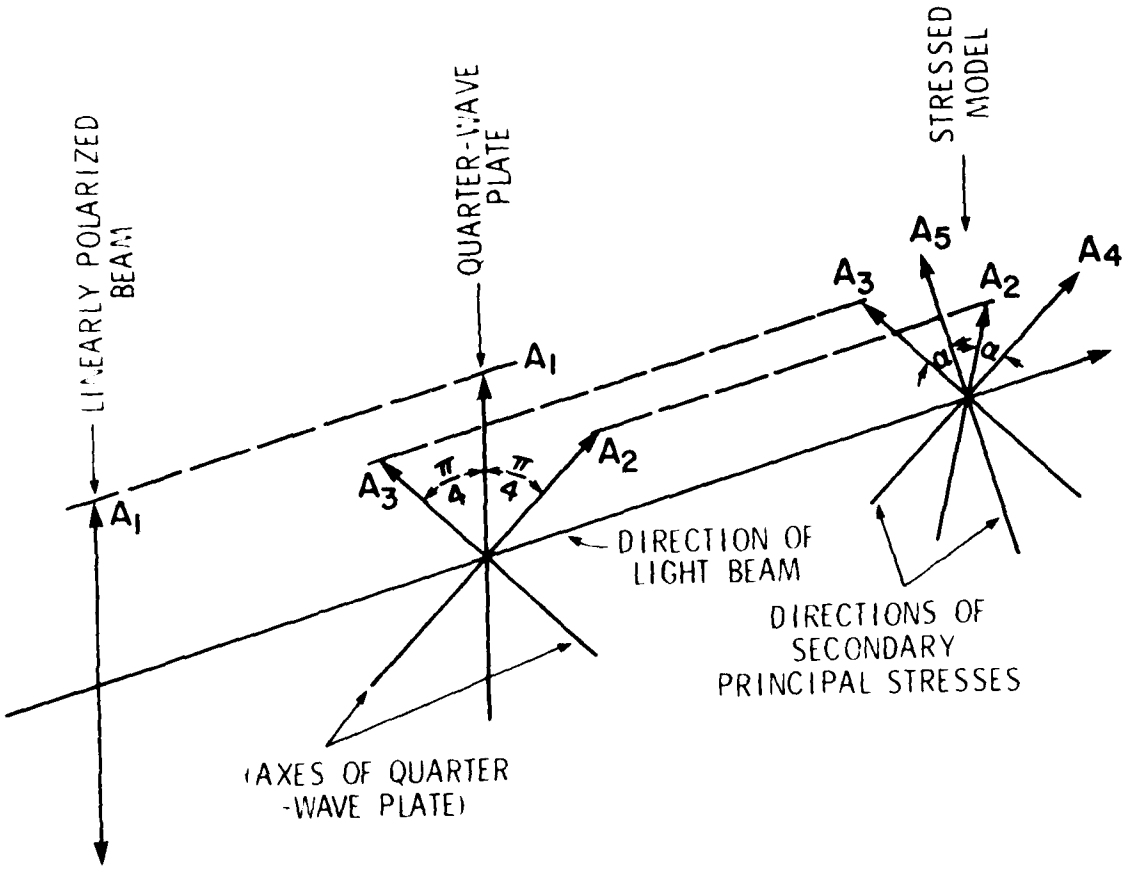

Figure 1. Transmission of a Linearly Polarized Light Beam through a Quarter-Wave Plate and a Stressed Model

If the secondary principal axes in a model make angles of "α" with the axes of the quarter-wave plate, A_2 and A_3 are resolved along these directions, giving components

$$A_4 = (2)^{-1/2} A \sin(\omega t - \alpha) \tag{4}$$

and

$$A_5 = (2)^{-1/2} A \cos(\omega t - \alpha + \phi) \tag{5}$$

where ϕ denotes the relative retardation between components.

It is known that the intensity of scattered light for a given direction of observation is proportional to the square of the apparent amplitude, which is defined as the amplitude of the component normal to the direction of observation. For observation along direction OA, which is collinear with the direction of polarization of the beam, OA_1, Figure 2, the component is given by

$$A_6 = A_4 \cos(\pi/4 - \alpha) - A_5 \sin(\pi/4 - \alpha)$$

$$A_6 \sin(\omega t + \phi_6) \tag{6}$$

where A_6 and ϕ_6 are the amplitude and the phase angle of the component, respectively. The intensity of the scattered light for this direction of observation is equal to $K_S(\bar{A}_6)^2$, where K_S is a material constant. It has been shown in Reference 13 that

$$K_S(\bar{A}_6)^2 = 1/2K_S A^2(1 + \cos 2\alpha \sin\phi) \tag{7}$$

Similarly, for observation along the direction OB, which makes an angle of $\pi/4$ radians with the direction OA, the component is given by

$$A_7 = A_4 \sin\alpha - A_5 \cos\alpha$$

$$= \bar{A}_7 \sin(\omega t + \phi_7) \tag{8}$$

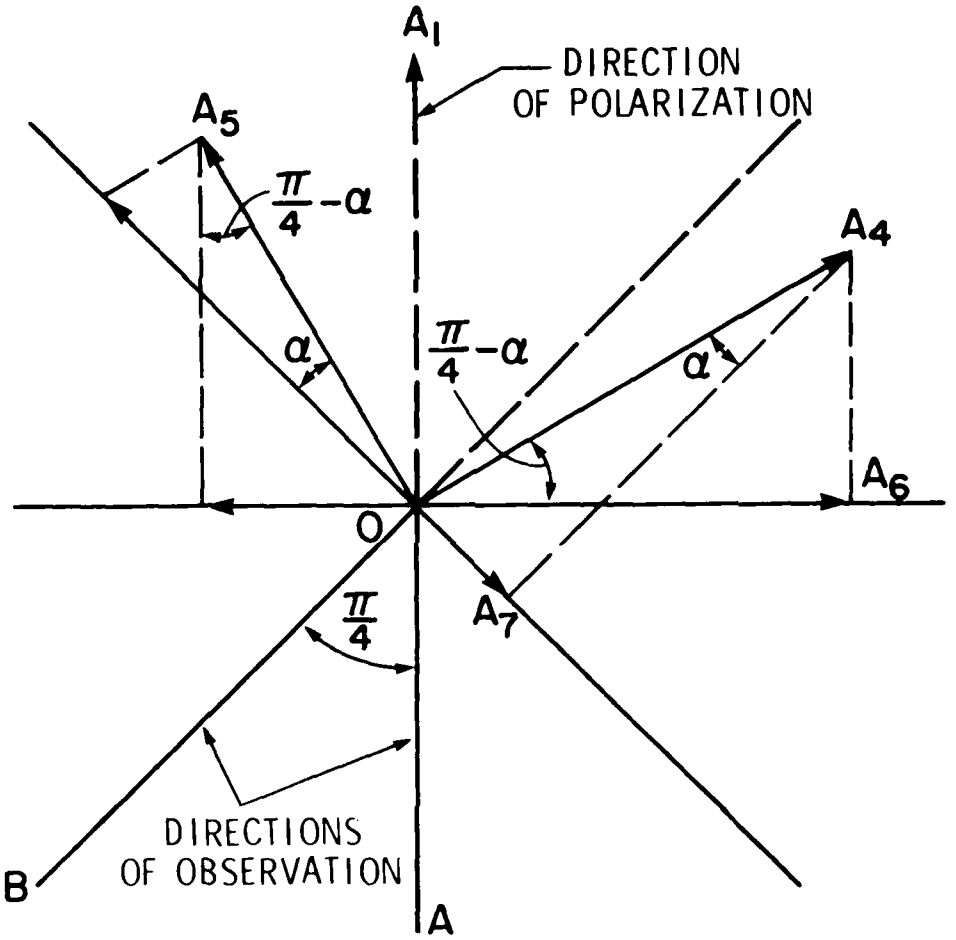

Figure 2. Directions of Observation OA and OB for Cases Without Rotation of Secondary Principal Axes. The light beam is pointed toward the reader from the plane of paper through point 'O'

where A_7 and ϕ_7 are the amplitude and the phase angle of the component, respectively. The intensity of scattered light for this observation is equal to

$$K_S(A_7)^2 = 1/2K_S A^2(1 + \text{Sin}2\alpha\ \text{Sin}\phi) \tag{9}$$

If the load is zero on the specimen,

$$K_S(\bar{A}_6)^2 = K_S(\bar{A}_7)^2 = 1/2K_S A^2 \tag{10}$$

because ϕ=0. Let U and V represent the ratio of the intensity of scattered light observed while the model is under load to that observed while it is free of load along the directions OA and OB, respectively (Reference 14).

$$U = K_S(\bar{A}_6)^2/2K_S A^2 = \left(\frac{\bar{A}_6}{A}\right)^2 \tag{11}$$

$$V = K_S(\bar{A}_7)^2/2K_S A^2 = \left(\frac{\bar{A}_7}{A}\right)^2 \tag{12}$$

At a point in the model

$$U = 1 + \text{Cos}2\alpha\ \text{Sin}\phi \tag{13}$$

$$V = 1 + \text{Sin}2\alpha\ \text{Sin}\phi \tag{14}$$

and

$$\alpha = 1/2\tan^{-1}\left[\frac{V-1}{U-1}\right] \tag{15}$$

$$\phi = \text{Sin}^{-1} \pm [(V-1)^2 + (U-1)^2]^{1/2} \tag{16}$$

Case II: Secondary Principal Axes Rotate

In the case of residual stresses, it is expected that the rotation of the secondary principal stresses are small and the errors due to the rotation of the secondary principal stresses can be neglected. Thus, for residual stress determination, the Case I theory will be assumed to apply.

2.2 SCATTERED-LIGHT PHOTOELASTIC PROPERTIES OF POLYCARBONATE AND ACRYLIC PLASTICS

A study of polycarbonate as a scattered-light photoelastic material is made in Reference 27. One of the principal advantages of scattered-light photomechanics is that passing a thin sheet of light through a model is equivalent to optically slicing the model without physically disturbing it. In order to do this it is necessary to immerse the model in a fluid having the same index of refraction as the model. This prevents the refraction of light when entering or leaving a curved surface in a three-dimensional model. Another requirement of an immersion fluid is that it shall not attack or degrade the model material within the time span of the testing and analysis. The index of refraction for polycarbonate is 1.58 and there are several immersion fluids whose index of refraction is very close to 1.58, such as Type IMF-1618 (Reference 36). Since the polycarbonate material is chemically attacked by many fluids, the immersion fluid should be enclosed in a thin walled transparent plastic container made of material having the same refractive index as the immersion fluid. Thus, the use of an immersion tank can be eliminated.

In addition to the requirement for compatibility with an immersion fluid, a model material must exhibit sufficient intensity of scattered light to permit use of this technique. Furthermore, the fringe density or number of fringes per inch must be enough to permit accurate analysis but not so much that the fringe pattern loses contrast to the point where individual fringes can no longer be resolved. Reference 27 reports the following fringe densities for polycarbonate in uniaxial tension: at the proportional limit, 110 fringes/inch; at a total strain of

5 percent, 375 fringes/inch; at 10 percent strain, 600 fringes/inch. These are high for a scattered-light model material. In our case, we are primarily interested in low levels of residual stresses. Therefore, this high fringe value may be an advantage.

The scattered-light properties of acrylic plastics were not reported in the literature review as a part of this program.

2.3 SCATTERED-LIGHT PHOTOELASTIC DEVICE

A typical scattered-light polariscope consists of the following elements (Figure 3, References 36 and 37):

2.3.1 Light Source and Light Conditioning System

The light source is a 15mw helium-neon laser, 632.8nm wavelength, complete with power supply and beam expander.

By means of the lens system L_1/L_2, one can choose between a "pencil" operation (light converging toward a point on the model) or a "ribbon" operation (light converging into a plane of "zero" thickness). A sliding indexed mount enables the selection of light desired (Slide A, Figure 3).

In order to obtain better photographic records and for easier observation of the fringe pattern, the "ribbon" of light can be expanded by manipulation of the lens system L_4/L_5 and L_6/L_7. The L_4/L_5 lens system expands the beam to 0.6 inches, and the L_6/L_7 lenses expand the beam to 1.5 inches.

The beam generated by the laser is plane polarized. Insertion of quarter-wave plates produces circular polarization. A second quarter-wave plate transforms the light back into plane polarization. The second quarter-wave plate is mounted in a rotatable mount, and its motion is indexed on a large graduated dial indicating the direction of emerging polarization.

The compensator 'C' is a Babinet-Soleil Digital Readout Uniform Field Compensator, with a calibrated counter.

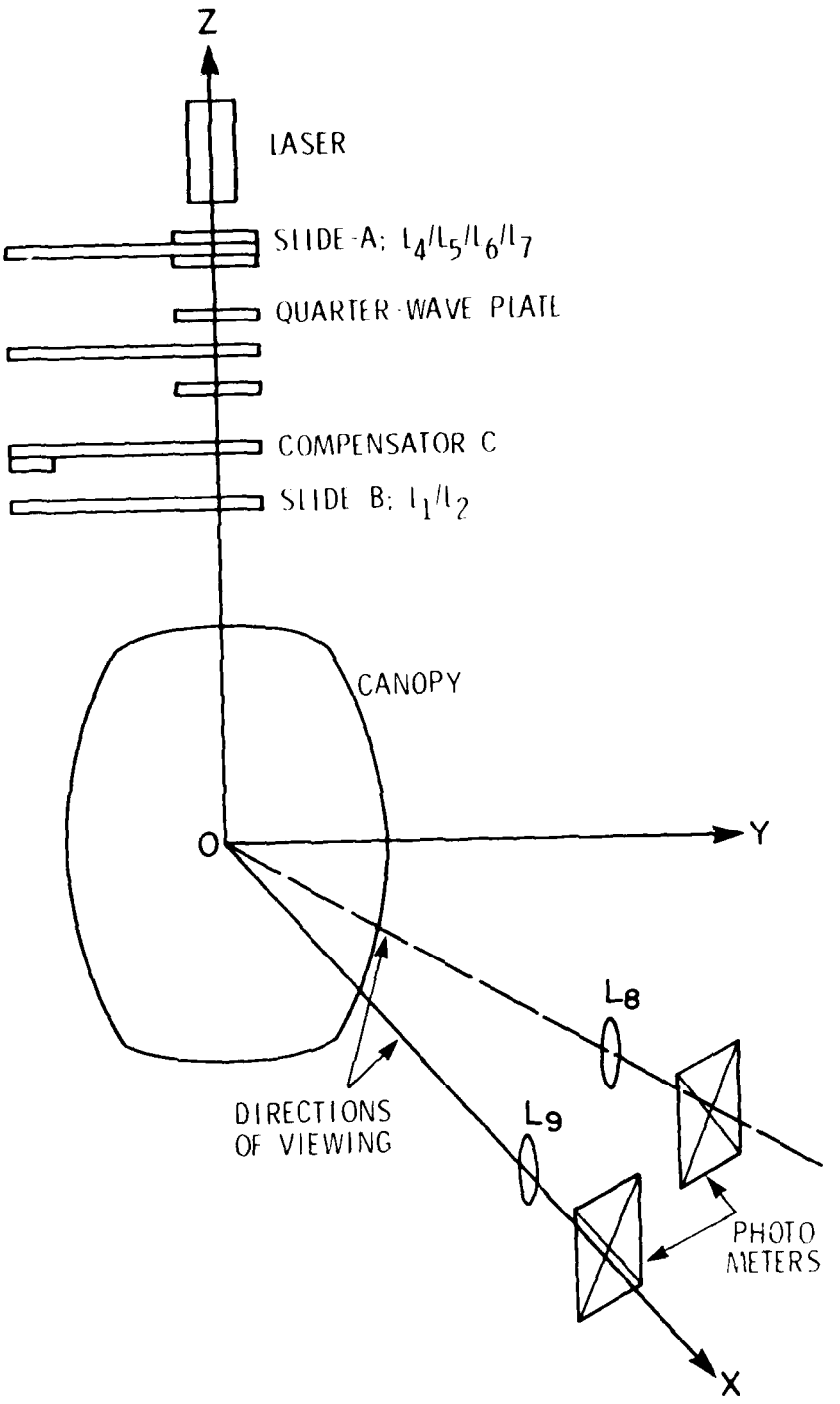

Figure 3. Elements of a Scattered-Light Polariscope.

The compensator is the heart of every polariscope measuring system, and its measuring accuracy determines the capability of the system.

2.3.2 Translation and Rotation Mechanism

There are two ways to design the translation and rotation mechanism. In the first case, we can keep the light source, conditioning system, and data acquisition system fixed and translate and rotate the model. In the second case, if the object is large, we can keep the test specimen fixed and translate and rotate light source, conditioning system, and the data acquisition system together. In the dual observation system used here, rotation of the model is not required, therefore, only x, y, and z translation of the light and data acquisition system together is to be accomplished.

The function of the translation mechanism is as follows: The x-y translation is used to select within the model lines of x-y coordinates to be analyzed. These motions are to be realized by precision slide mechanisms and the corresponding displacements are readable to an accuracy of 0.001 inch or 0.025 mm. Once the x-y coordinates are selected, the analysis along a line is carried out point-per-point using "z" motion.

For separation of principal stresses in the scattered light technique, the shear difference method must be used. Therefore, measurement of the displacements x-y are important and directly influence the accuracy of results obtained.

2.3.3 The Data Acquisition System

The data acquisition system is used to collect the photoelastic information from the model being analyzed. Three different methods of acquiring the data are provided. They are (Figure 4):

- Visual - The photoelastic pattern is directly observed on a ground glass screen.

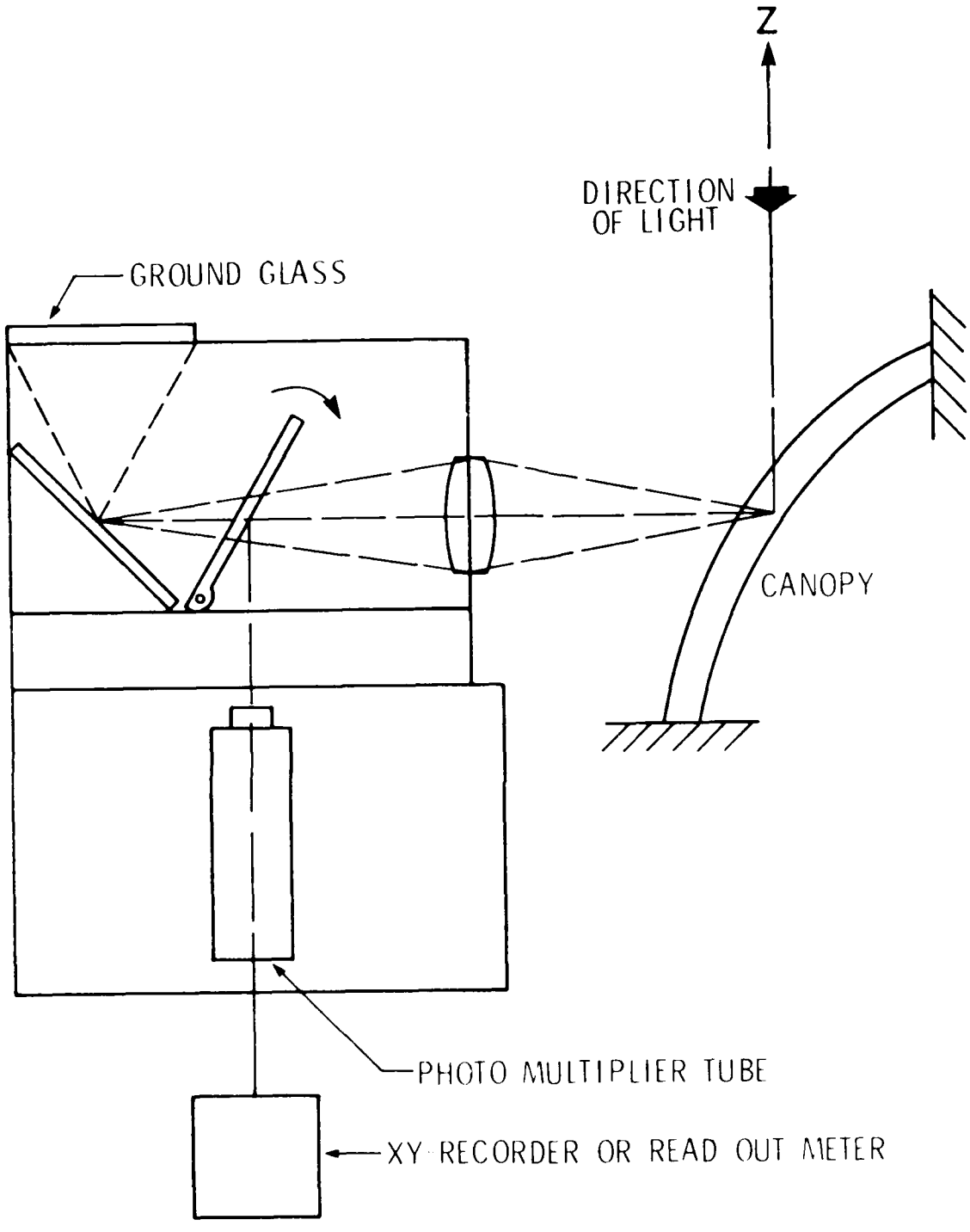

Figure 4. Scattered-Light Data Acquisition System.

- Photographic - A photographic record of the observed pattern is made on a 35-mm film.

- Photoelectric - A photomultiplier tube is incorporated in the data acquisition system which provides an electrical output proportional to the light intensity emerging from the observed pattern. The distance between fringes is very accurately determined by photoelectric measurement. The light intensities are measured either on a meter or recorded on an x-y plotter.

2.4 PROCEDURE TO DETERMINE THE RESIDUAL STRESSES

Consider Figures 5(a, b, and c) and 6(a, b, c, and d). By sending the incident light beam in a direction parallel to z-axis and making scattered light observations in the xy-plane, one can get the secondary principal stress difference (p' - q') in the xy-plane as well as the directions of p' and q'. If :' is the orientation of the p'-stress with respect to the y-axis, N is the fringe value and $\bar{C}$ is the stress-optic coefficient.

$$p' - q' = \left(\frac{dN}{dz}\right) \bar{C} \tag{17}$$

$$\tau_{yx} = \frac{p' - q'}{2} \text{Sin}2:'$$

and

$$(\ _y - \ _x) = (p' - q')\text{Cos}2:' \tag{18}$$

Similarly, in Figure 5(b) the light beam is in the y-direction and viewing is in the xz-plane. From this we can determine $\ _{zx}$ and $\ _z - \ _x$.

$$p'' - q'' = \frac{dN}{dy} \cdot \bar{C} \tag{19}$$

$$\tau_{xz} = \frac{p'' - q''}{2} \text{Sin}2:''$$

$$\ _z - \ _x = (p'' - q'')\text{Cos}2:'' \tag{20}$$

Similarly, from Figure 5(c) we can determine $\ _{zy}$ and $\ _z - \ _y$.

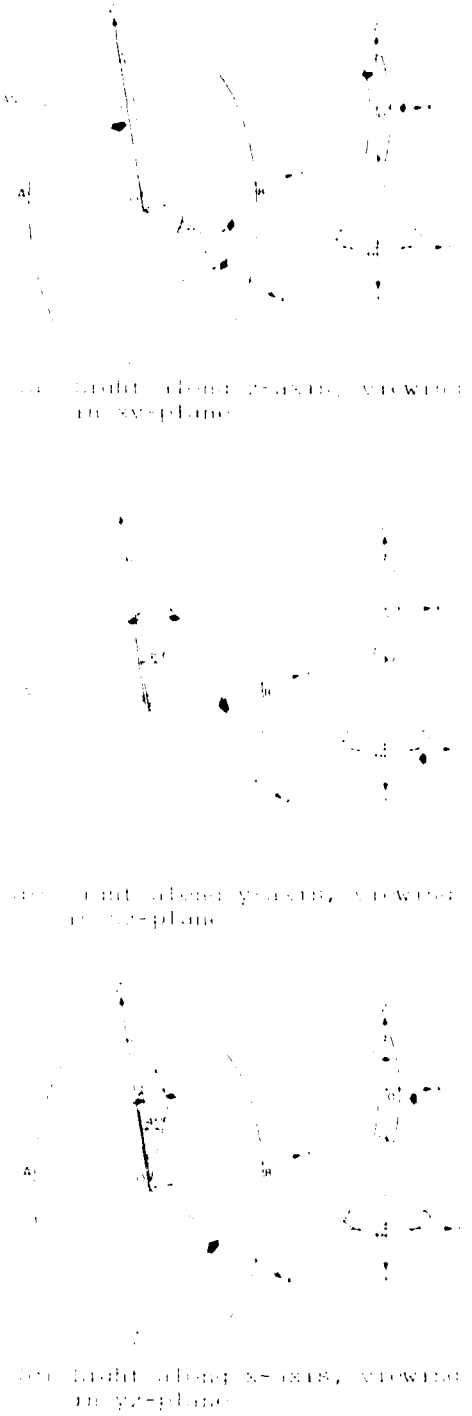

Figure 5. Directions of Light and Viewing in a Canopy.

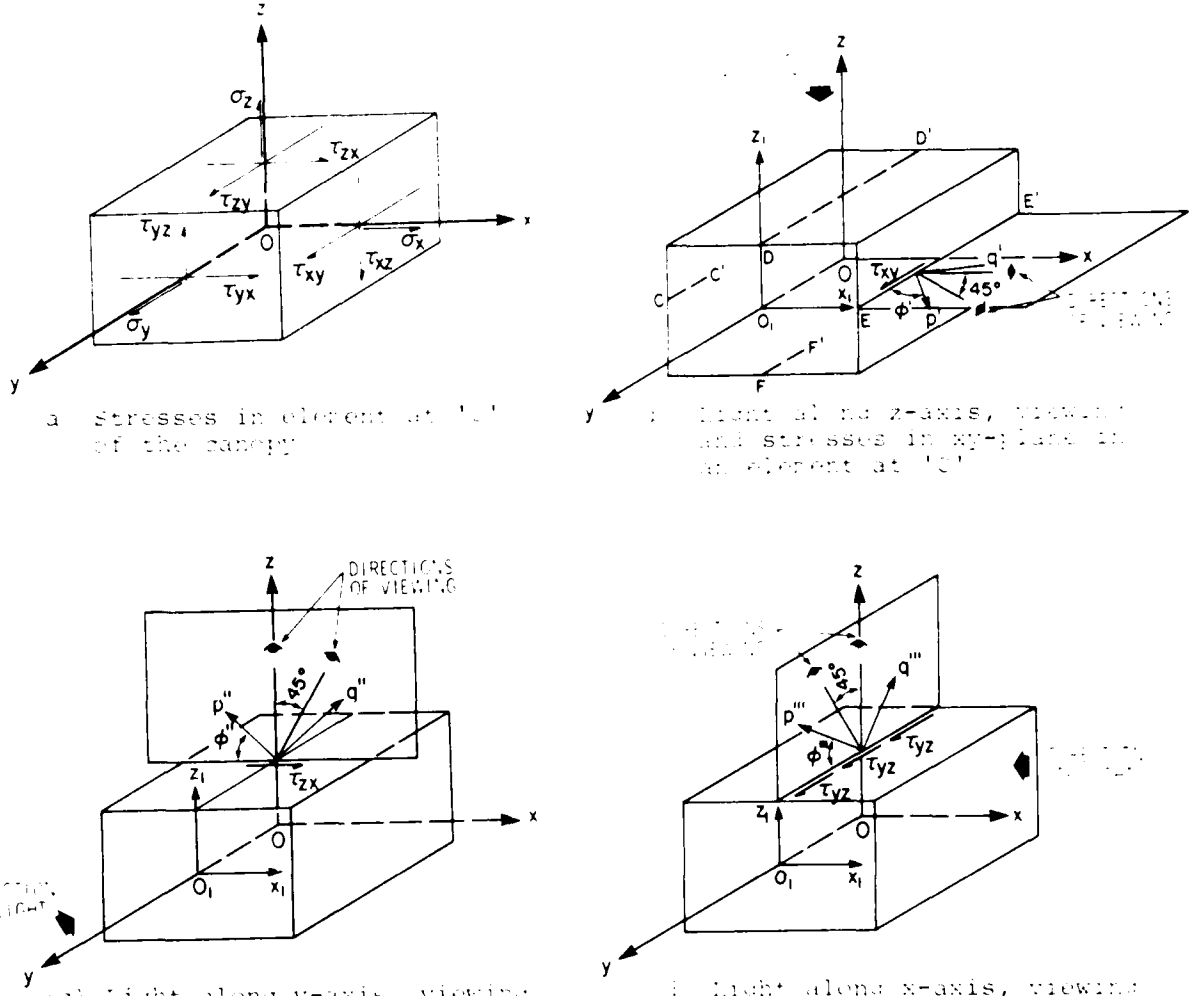

a Stresses in element at 'O' of the canopy

b Light along z-axis, viewing and stresses in xy-plane in an element at 'O'

c Light along y-axis, viewing and stresses in xz plane

d Light along x-axis, viewing and stresses in y-z plane in an element at 'O'

Figure 6. Directions of Light, Viewing and Stresses in an Element at 'O'.

In order to determine the individual normal stresses, recourse is to be made to the shear difference method. Thus, let it be required to determine the normal stress components along the y-axis, Figure 6(b). For this purpose we will use the equation of equilibrium, namely

$$\frac{\Delta \tau_{yx}}{\Delta x} + \frac{\Delta \sigma_y}{\Delta y} + \frac{\Delta \tau_{yz}}{\Delta z} = 0 \qquad (21)$$

From this, using finite differences, we integrate the equations numerically,

$$(\sigma_y)_j = (\sigma_y)_F - \sum_f^j \frac{\Delta \tau_{yx}}{\Delta x}\Delta y + \sum_f^j \frac{\Delta \tau_{yz}}{\Delta z}\Delta y \qquad (22)$$

in which $(\sigma_y)_j$ denotes the value of σ_y at any point j along the y-axis and $(\sigma_y)_F$ is the known or the initial value at some point F; for example, at a free surface $(\sigma_y)_F = 0$.

The values of $\frac{\Delta \tau_{yx}}{\Delta x}$ are obtained from the shear τ_{yx} along two parallel lines Δx apart such as lines CC' and EE', Figure 6(b). Similarly, the values of $\frac{\Delta \tau_{yz}}{\Delta z}$ are obtained from the shears τ_{yz} along such lines as DD' and FF', Δz apart. These give us the necessary data for the evaluation of σ_y at all points along the y-axis. σ_x is solved from Equation 18. The component of shear stress "τ_{zy}" is determined by passing the light in the direction of x-axis and viewing in yz-plane (Figures 5(c) and 6(d)). By a knowledge of all six stress components, we can get the principal stresses at a pont by Mohr's Circle or from the principal stress equations.

2.4.1 Surface-Stress Determination

One technique in examining boundary surfaces for critical points is to traverse the surface with the circularly polarized beam intersecting the boundary at right angles (along N) and recording the fringe pattern, Figure 7 A flexible coherent-fiber optics tube would be convenient here. When the light beam

is along a principal direction as in this case, the stress-optic law reveals the difference in the other two secondary principal stresses (Figure 8(a)):

$$p^* - q^* = \left(\frac{d\bar{N}}{dN}\right)\bar{C} \tag{23}$$

$$\tau_{yx} = \frac{p^* - q^*}{2} \sin 2\phi^*$$

$$\sigma_x - \sigma_y = (p^* - q^*)\cos 2\phi^* \tag{24}$$

To obtain the third independent bit of information, let the laser light intersect the point of interest at an angle (along N'), Figure 7, in the xz-plane. The direction Cosines of N, one of the secondary-principal stress directions, are

$$\ell_1 = \cos\gamma$$

$$m_1 = 0 \tag{25}$$

$$n_1 = -\sin\gamma$$

The scattered-light photoelastic pattern is sufficient to yield, (Figure 8(b))

$$\bar{C}\left(\frac{d\bar{N}}{dN'}\right) = \bar{+}(p^{**} - q^{**}) \tag{26}$$

$$\tau_{yN} = \frac{(p^{**} - q^{**})}{2} \sin 2\phi^{**}$$

$$(\sigma_N - \sigma_y) = (p^{**} - q^{**})\cos 2\phi^{**} \tag{27}$$

It should be noted that if z is chosen to be exactly normal to the surface, then it becomes one of the principal stress directions. p* and q* are then the other 2 principal stresses, otherwise they will be the secondary principal stresses.

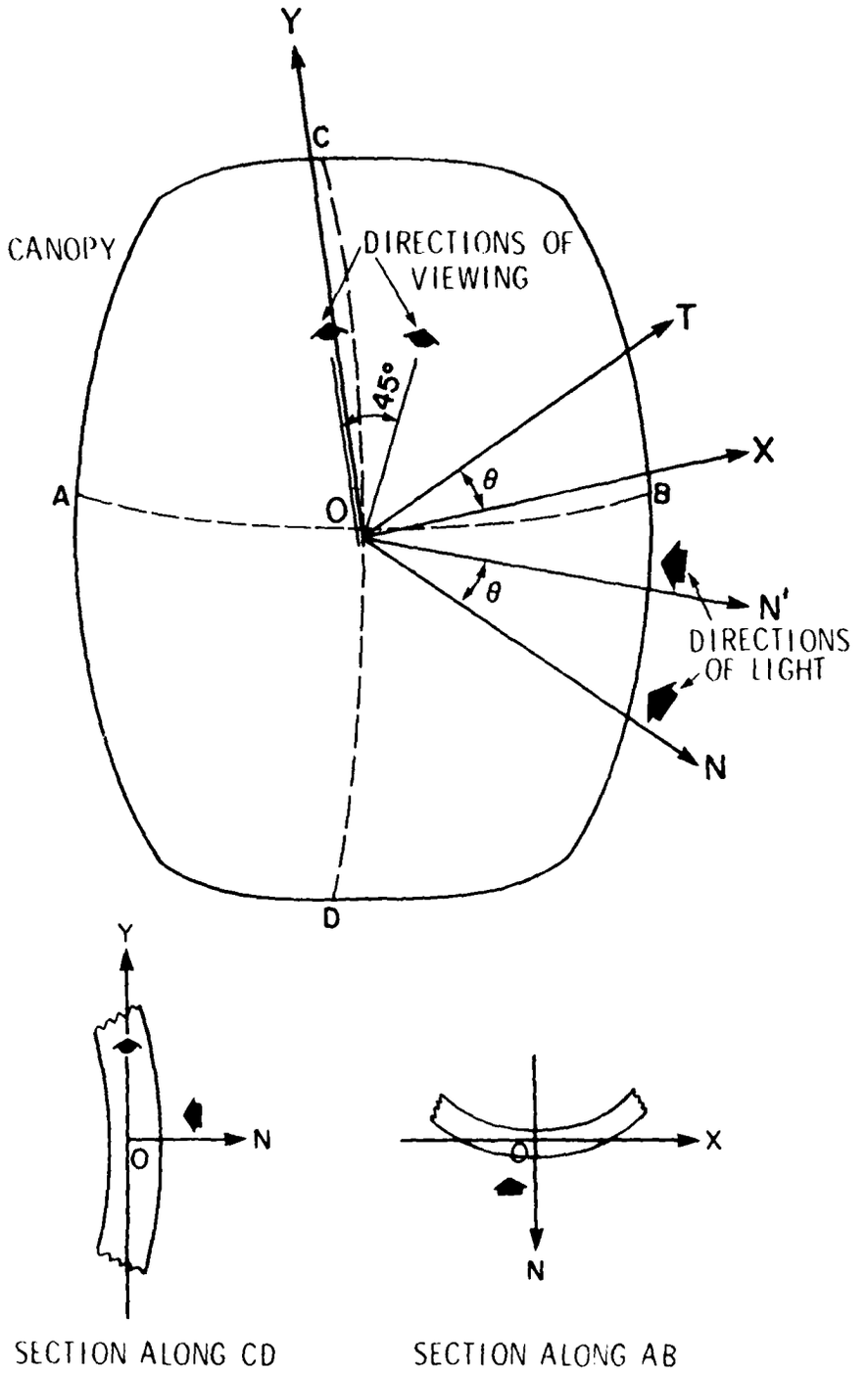

Figure 7. Light Along N and N' Axes, Viewing in xy and Ty Planes in Canopy.

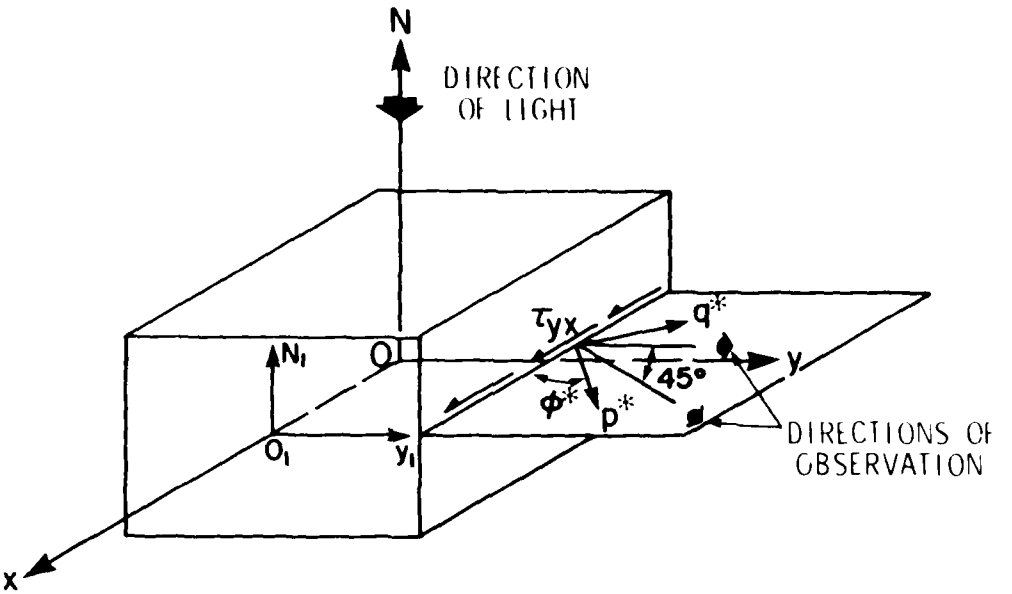

(a) Light along N-axis, viewing and stresses in xy-plane an element at 'O'

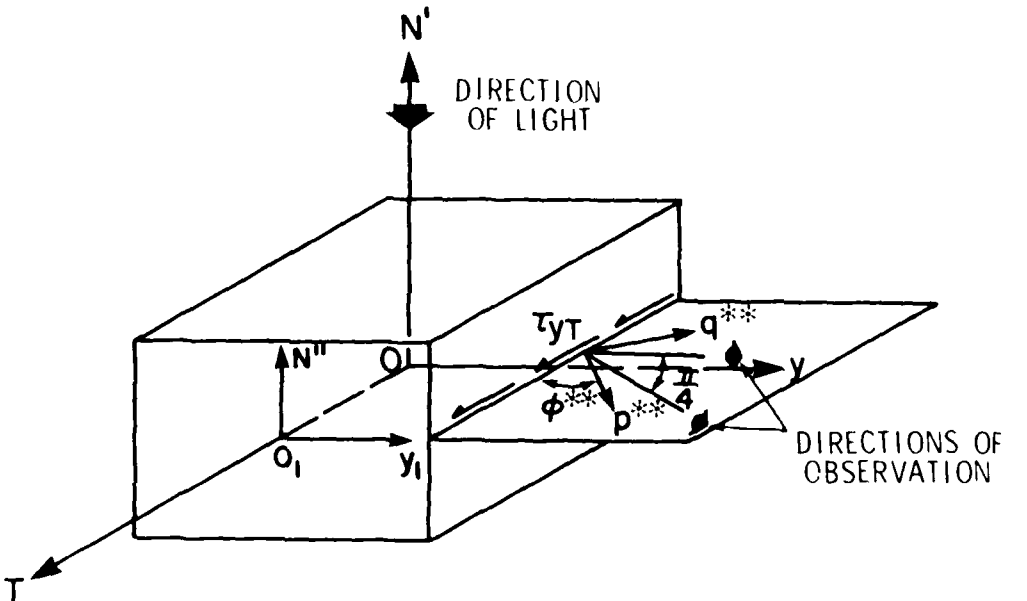

(b) Light along N'-axis, viewing and stresses in Ty-plane

Figure 8. Directions of Light, Viewing, and Stresses in an Element at 'O'.

By transformation of coordinates

$$\sigma_N = \sigma_x \ell_1^2 + \sigma_y m_1^2 + \sigma_z n_1^2 + 2\sigma_{xy} \ell_1 m_1 + 2\sigma_{xz} \ell_1 n_1 + 2\sigma_{yz} m_1 n_1 \quad (28)$$

Because the point of interest is on the boundary,

$$\sigma_{xz} = \sigma_{yz} = \sigma_z = 0 \quad (29)$$

therefore

$$\sigma_N = \sigma_x \cos^2 \theta \quad (30)$$

Equation 26 takes positive values if $\sigma_N > \sigma_y$ and a negative value if $\sigma_N < \sigma_y$. Solving Equations 24, 27, and 30, we can determine individually σ_x, σ_y, and τ_{xy}. Since we know the directions of secondary principal stresses, namely ϕ^* and ϕ^{**}, we can determine the values of principal stresses at the boundary surface.

2.5 APPROXIMATE COST OF SCATTERED-LIGHT DEVICE

(a) *Light Source and Conditioning System* Consisting of 15 mW Helium-Neon Laser, 632.8 nm Wavelength, Complete with Power Supply and Beam Expander

The light conditioning unit consists of several lens systems to provide a "ribbon" or "pencil" of light (light converging toward the data point within the model), or 0.75 in. (19 mm) "ribbon" of light (light converging into a plane of "zero" thickness). A sliding indexed mount enables easy selection of the desired light operation. Another set of lenses provides for the widening of the ribbon of light to 1.5 in. (38 mm) to obtain better photographic records. The light conditioning system should provide

A. Plane Polarization, with readout to 1/2°.

B. Circular Polarization.

C. Babinet-Soleil Compensation, calibrated to 1/100 fringe. Total range 5 fringes.

Cost Estimate: $33,340

(b) Fixture for Translation of Light and Viewing System

This fixture should provide for X-Y-Z displacement of the light and viewing system. The displacements are readable to 0.001 in. (0.025 mm), the fixture should feature a 6 in. (152 mm) X, Y, Z travel.

Cost Estimate: $15,360

(c) Data Acquisition System

Data acquisition system consisting of a photomultiplier tube with a readout

Cost Estimate: $24,600

(d) Index Matching Fluid

Five-gallon containers indexing matching fluid, IMF-1618A

Cost Estimate: $645

Total Cost $[illegible],945

The costs shown in items (a) and (c) are based on the quotation (dated July 1982) from Photoelastic Division, Measurements Group. The cost shown in (b) is an estimate, as there is no readily available system to simultaneously translate the light and viewing system and to measure these translations in a predetermined X, Y, and Z coordinate system.

SECTION 3

ULTRASONIC TECHNIQUE I
(RAYLEIGH SURFACE WAVES)

In 1885, the English scientist Lord Rayleigh (Reference 60) demonstrated that waves can be propagated over the plane boundary between an elastic half-space and a vacuum or a sufficiently rarefied medium (for example, air), where the amplitude of the waves decays rapidly with depth. During the last fifteen years, Rayleigh waves in the ultrasonic frequency range have found considerable application. They can be used to inspect the state of the surface layer of a sample, in the detection of surface and near-surface defects in metals, glasses, and plastics, and other materials (ultrasonic surface flaw detection). The influence of the properties of the surface layer of a sample on the velocity and attenuation of Rayleigh waves permits the latter to be used for the assessment of residual stresses in a surface layer of a material, as well as the thermal and mechanical properties of the surface layer of a sample.

3.1 PRINCIPLES AND ANALYSIS

3.1.1 The Concept of Rayleigh Waves: Their Structure and Properties

Let us consider a plane harmonic Rayleigh wave on the boundary between a solid, isotropic, perfectly elastic half-space and vacuum. Let the half-space occupy the region $Z > 0$ (Figure 9(a)), the direction of wave propagation coinciding with the X-axis. For the region occupied by the half-space, we introduce the scalar potential $\overline{\varphi}$ and vector potential $\overline{\psi}$ of the displacements, so that the particle displacement vector $\dot{v}$ is written in the form

$$\dot{v} = \text{grad}\ \overline{\varphi} + \text{rot}\ \overline{\psi} \qquad (31)$$

The potentials $\overline{\varphi}$ and $\overline{\psi}$ are the potentials of the longitudinal and shear waves, respectively, and satisfy the following wave equation:

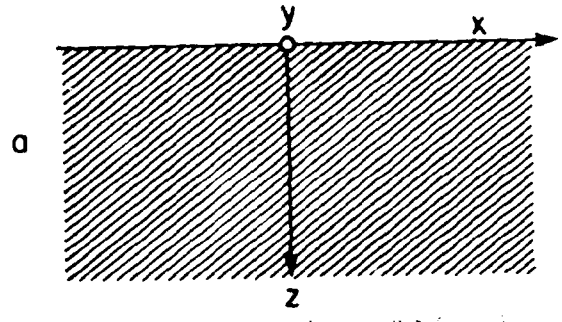

Elastic media : $z > 0$
Vacuum : $z < 0$

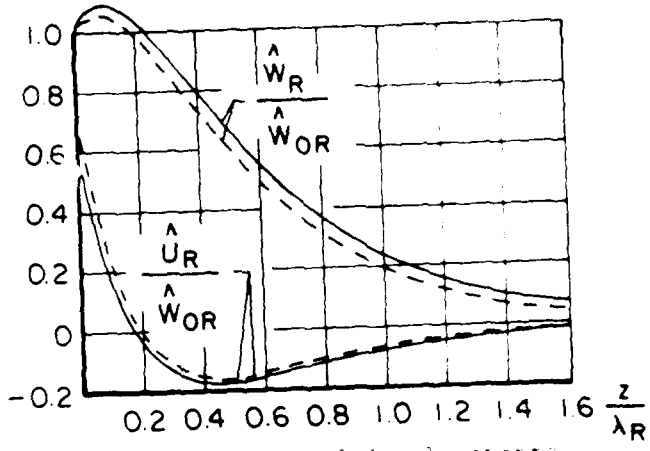

Dependence of displacements on the depth

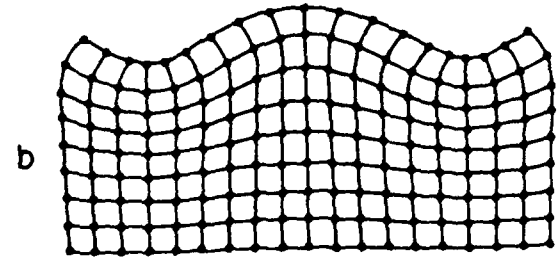

Displacements due to Rayleigh waves

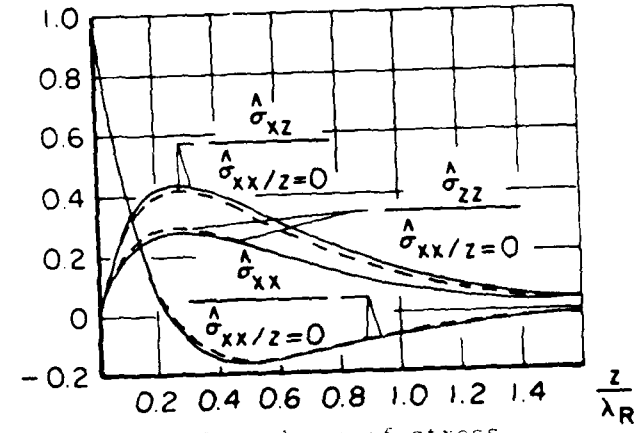

Dependence of stress amplitudes on depth

Figure 9. Displacements and Stresses due to Rayleigh Waves.

$$\frac{\partial^2 \phi}{\partial x^2} + \frac{\partial^2 \phi}{\partial z^2} + K_\ell^2 \phi = 0$$

$$\frac{\partial^2 \psi}{\partial x^2} + \frac{\partial^2 \psi}{\partial z^2} + K_t^2 \psi = 0 \qquad (32)$$

Here,

$$K_\ell = \omega \sqrt{\rho_0 / (\lambda + 2\mu)}$$

$$K_t = \omega \sqrt{\rho_0 / \mu} \qquad (33)$$

are the wave numbers for longitudinal and transverse modes, respectively, ω is the circular frequency, λ and μ are Lamé elastic constants, and ρ_0 is the mass density of the medium.

The components U and W of the particle displacement along the x and z axes, respectively, and the stress components σ_{xx}, σ_{zz}, σ_{xz} may be represented in terms of $\bar{\phi}$ and $\bar{\psi}$ according to the equations

$$U = \frac{\partial \phi}{\partial x} - \frac{\partial \psi}{\partial z}$$

$$W = \frac{\partial \phi}{\partial z} + \frac{\partial \psi}{\partial x} \qquad (34)$$

$$\sigma_{xx} = \lambda \left(\frac{\partial^2 \phi}{\partial x^2} + \frac{\partial^2 \phi}{\partial z^2} \right) + 2\mu \left(\frac{\partial^2 \phi}{\partial x^2} - \frac{\partial^2 \psi}{\partial x \partial z} \right)$$

$$\sigma_{zz} = \lambda \left(\frac{\partial^2 \phi}{\partial x^2} + \frac{\partial^2 \phi}{\partial z^2} \right) + 2\mu \left(\frac{\partial^2 \phi}{\partial z^2} + \frac{\partial^2 \psi}{\partial x \partial z} \right) \qquad (35)$$

$$\sigma_{xz} = \mu \left(2 \frac{\partial^2 \phi}{\partial x \partial z} + \frac{\partial^2 \psi}{\partial x^2} - \frac{\partial^2 \psi}{\partial z^2} \right)$$

We seek the solutions to Equations 32 corresponding to a plane harmonic wave propagating in the positive x direction. For this we let

$$\psi = F(z)\, e^{i(kx-\omega t)}$$
$$\chi = G(z)\, e^{i(kx-\omega t)} \tag{36}$$

Substituting these expressions into Equations 33, we obtain two differential equations for the functions F(z) and G(z):

$$\frac{d^2F(z)}{dz^2} - (k^2 - k_\ell^2)\, F(z) = 0$$
$$\frac{d^2G(z)}{dz^2} - (k^2 - k_t^2)\, G(z) = 0 \tag{37}$$

The two linearly independent solutions of each of the above equations are the $\exp(\pm\sqrt{k^2-k_\ell^2}\,z)$ and $\exp(\pm\sqrt{k^2-k_t^2}\,z)$. We assume $k^2 > k_t^2 > k_\ell^2$. Then the solutions with postiive radicals in the exponent will correspond to motion increasing with depth, the solution with negative radicals will correspond to exponentially decaying motion, i.e., a surface wave. Consequently, the expressions for ψ and χ assume the form

$$\psi = A\, e^{-qz}\, e^{i(kx-\omega t)}$$
$$\chi = B\, e^{-sz}\, e^{i(kx-\omega t)} \tag{38}$$

where

$$q^2 = k^2 - k_\ell^2$$
$$s^2 = k^2 - k_t^2 \tag{39}$$

and A and B are arbitrary constants.

The conditions of the problem demand also that the stresses σ_{zz} and σ_{xz} go to zero at the boundary of the half-space (plane z = 0).

The pattern of the displacements in a Rayleigh wave is illustrated in Figure 9(b). Figures 9(c) and 9(d) show the dependence of the displacement amplitudes $\hat{U}_R$, $\hat{W}_R$ and stress

amplitudes σ_{zz}, σ_{xx}, σ_{xz} in a Rayleigh wave on the depth. The curves are given in dimensionless form; the displacement amplitudes are referred to the normal displacement amplitude on the surface W_{OR}, the stress amplitudes are referred to the amplitude $\sigma_{xx} \neq 0$ on the surface. The set of curves shown in Figure 9(c) and 9(d) illustrates the localization of the Rayleigh wave in a thin surface layer of thickness λ_R to $2\lambda_R$.

3.1.2 Propagation of Rayleigh Waves in a Stressed Elastic Medium

For the measurement of stress, the effect of higher order elastic constants on the velocity of Rayleigh and shear waves in a material must be considered. An initially isotropic material which has been subjected to any stress system other than hydrostatic pressure will become anisotropic, and the velocity of ultrasonic waves generated through it will become nondegenerate. In order to make reference to an initially isotropic stress-free body (Reference 39), it is necessary to refer the body to a set of three orthogonal axes. The three axes describing the elastic nature of the body correspond to the three principal stress axes.

For a material in a general stressed state, the nature of any wave propagated along any of the principal strain axes is either of a pure longitudinal or pure transverse nature. These are the "principal waves" and they travel along the "acoustic axes." This can be explained by the fact that for an isotropic material there is complete degeneracy, and the material has no preferred direction of its own. A wave propagated through the material will travel in any direction with the same velocity. The ultrasonic wave traveling through a material in any direction can, besides this direction, recognize only the direction of the principal axes in the material and these correspond to a set of orthogonal axes, coincident with the principal stresses. These are the three principal directions which can influence the velocity of the ultrasonic wave in the material. For the case where the principal strains are all distinct and unlike, each

axis can support three ultrasonic waves--one longitudinal and two transverse--and there are a total of nine possible principal waves in the material. These waves may be described in terms of their directions of propagation and particle displacement. A transverse wave has its propagation direction parallel to one of the principal axes and its particle displacement along either of the other two principal axes.

3.1.2.1 Stress-Velocity Expressions (Uniaxial Stress Field)

Expressions have been derived by Hughes and Kelly in Reference 49 for the stress dependence of the velocities of ultrasonic waves along the principal stress axes using formulations of finite strain. The expressions relate to waves in initially isotropic materials and relate to the simple case of uniaxial stress. Figure 10 shows the coordinate system used for defining the propagation direction. The equations are given by

$$\rho_o V^2_{sy} = \rho_o V^2_{sz} = \mu + \frac{T}{3K_o}\left[4\lambda + 4\mu + m + \left(\frac{\lambda}{2} \times \frac{n}{4}\right)\right]$$

where uniaxial tension acts in the x-direction

$$\rho_o V^2_{sy} = \mu + \frac{T}{3K_o}\left[\lambda + 2\mu + m + \left(\frac{\lambda}{2} \times \frac{n}{4}\right)\right] \qquad (40)$$

$$\rho_o V^2_{sz} = \mu - \frac{T}{3K_o}\left[2\lambda - m + \frac{n}{2} + \left(\frac{\lambda}{2} \times \frac{n}{2}\right)\right]$$

where uniaxial tension T acts in y-direction

V_{sy}, V_{sz} = velocities of the shear waves polarized in y,z directions

λ and μ = second-order Lamé constants for isotropic materials

m and n = Murnaghan third-order elastic constants for isotropic materials, and

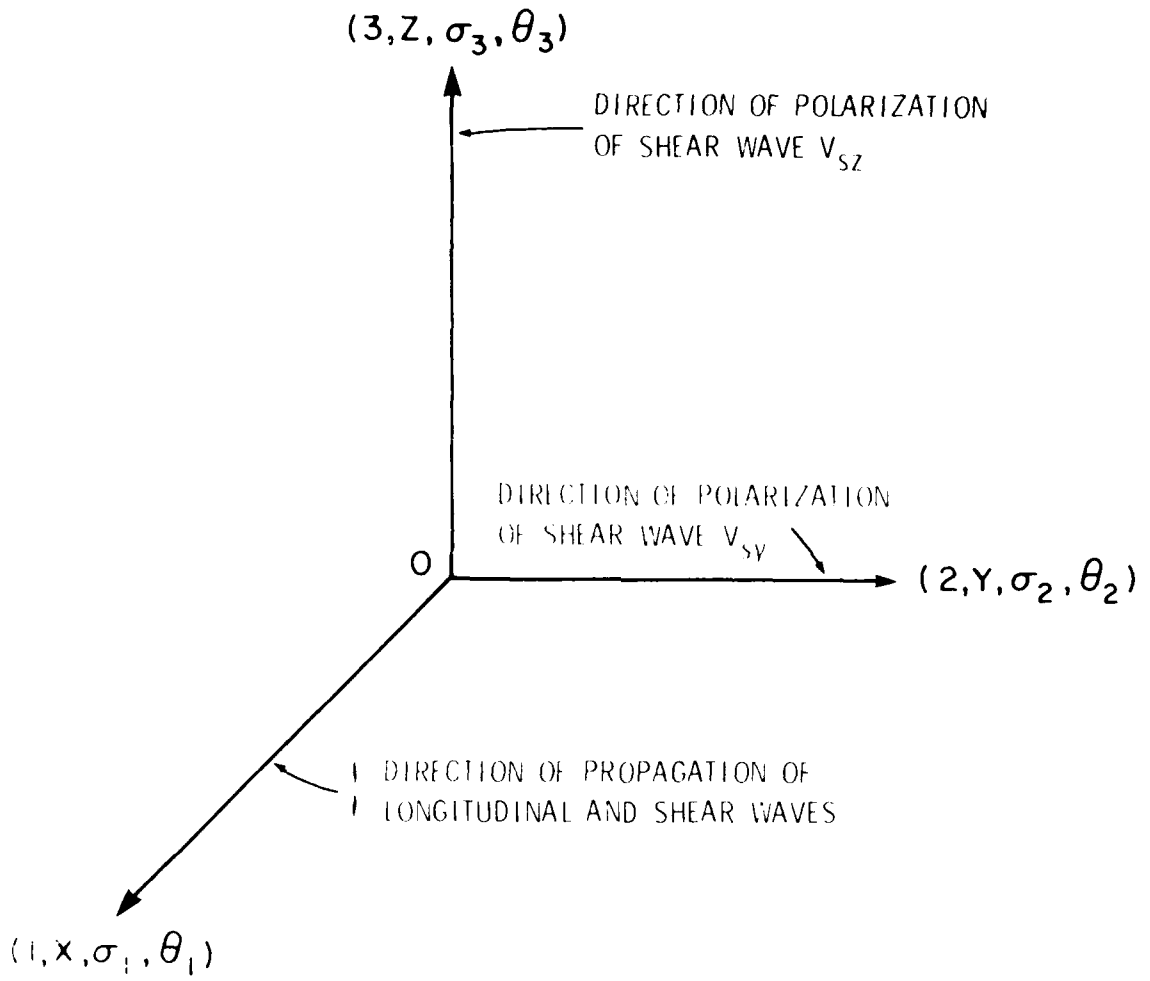

Figure 16. Directions of Coordinates Defining Propagation and Polarization of Shear Waves; Principal Stresses and Stretches.

$K_o = \frac{1}{3}(3\lambda + 2\mu)$ = bulk modulus

x = direction of propagation of waves.

It is readily seen that on reducing the uniaxial tension T to zero, the expressions reduce to the common form for the velocity V_{so} of the ultrasonic waves in an unstrained isotropic material, given by

$$\rho_o V^2_{s\,\cdot} = \mu \qquad (41)$$

This well-known expression is easily derivable from the theory of first-order elasticity where infintesimal strains are considered. If the sign of the T is changed from plus to minus, then this equation gives the velocities V_{sy} and V_{sz} as a function of uniaxial compressive stress.

From the transverse-wave velocity for the stress-free case, V_{so} ($= \sqrt{\mu/\rho_o}$), one can obtain the Rayleigh wave velocity, V_{Ro}, from the Bergmann approximation (which is appropriate for isotropic materials) (Reference 41)

$$V_{Ro} \quad \left[\frac{0.87 + 1.12}{1 + } \right] V_{so} \qquad (42)$$

where ($\frac{}{2(\quad)}$) is Poisson's ratio. It is assumed that for the stressed state ($T \neq 0$), the Bergmann approximation is still valid. In the stressed state, Poisson's ratio would contain third-order elastic constants in addition to the second-order constants. Since this relation is not known, it will be assumed that, as a first approximation, the ratio of elastic constants changes negligibly. Thus we have

$$V_R = \left[\frac{0.87 + 1.12}{1 + } \right] V_s \qquad (43)$$

where V_s has already been known.

3.1.2.2 Stress-Velocity Expressions (General Stress Field)

In Reference 63, expressions are derived for the speed of propagation of transverse waves in a body with an

arbitrary, homogeneous body with arbitrary stress field, on the basis of a general theory of elasticity formulated by Truesdell.

Taking the linear elastic theory as the basis for a derivation of the velocity V_{so} of a transverse wave in a homogeneous, isotropic body, we find

$$V_{so} = \sqrt{\frac{\mu}{\rho_o}} \tag{44}$$

where μ is a Lamé constant and ρ_o is the density. V_{so} is thus independent of stress in the body if ρ_o is constant.

A nonlinear theory must therefore be used to explain the stress-velocity relationship in a propagating stress wave. Truesdell has derived the following general results on the basis of such a theory.

(1) Three independent waves can propagate along any direction in an elastic material with a given strain field. The directions of the vectors describing the waves are designated the acoustic axes.

(2) The acoustic axes form a triad, the orientation of which depends on (a) the direction of propagation of the wave, (b) the direction of the axes of symmetry of the material, (c) the direction of the principal stresses, and (d) the directions of the principal strains.

(3) In an isotropic material, the orientation of the acoustic axes depends only on the direction of propagation and the directions of the principal stresses because the symmetry axes of the material are arbitrary and the axes of the principal stresses coincide with those of the principal strains.

(4) If the wave propagates along the direction of a principal stress, the acoustic axes will coincide with the principal stress axes. In this case, and this case only, pure longitudinal or transverse waves are propagated.

(5) The speed of propagation of pure transverse waves can be expressed by:

$$\frac{\rho V_{12}^2}{\theta_1^2} = \frac{\sigma_1 - \sigma_2}{\theta_1^2 - \theta_2^2}$$

$$\frac{\rho V_{13}^2}{\theta_1^2} = \frac{\sigma_1 - \sigma_3}{\theta_1^2 - \theta_3^2} \qquad (45)$$

where ρ is the density in the deformed state, V_{12} and V_{13} are the speeds of propagation for a transverse wave propagating along the direction of the first principal-stress axis and polarized along the directions of the second and third principal-stress axes, respectively, and σ_1, σ_2, and σ_3 are principal stresses, and θ_1, θ_2, and θ_3 are principal stretches (Figure 10).

Truesdell also shows that the expressions in Equation 45 can be transformed into the following in a second-order theory of elasticity.

$$\frac{\rho_o V_{12}^2}{\mu} = 1 + 2\delta_1 + (1+\frac{1}{2}\epsilon_5)(\delta_1+\delta_2+\delta_3) + \frac{1}{2}\epsilon_6(\delta_1+\delta_2)$$

$$\frac{\rho_o V_{13}^2}{\mu} = 1 + 2\delta_1 + (1+\frac{1}{2}\epsilon_5)(\delta_1+\delta_2+\delta_3) + \frac{1}{2}\epsilon_6(\delta_1+\delta_3) \qquad (46)$$

where δ_1, δ_2, and δ_3 are principal extensions, ϵ_5 and ϵ_6 are second order elasticity constants, and ρ_o is the mass density in the undeformed state.

The Equations 46 are derived assuming that δ_i $(i=1,2,3)$ is small, so that terms containing δ_i^2 can be neglected. This means that δ_i can be approximated by the principal values E_i in the strain tensor E. In Truesdell's expressions (Equation 46), Hooke's law can be introduced in the following form:

$$\varepsilon_i = E_i - \frac{\lambda}{2\mu(3K_o)} (\sigma_1+\sigma_2+\sigma_3) + \frac{1}{2\mu}\sigma_1 \qquad (47)$$

where i = 1,2,3 and λ and μ are the Lamé constants, $K_o = \frac{1}{3}(3\lambda+2\mu)$ is the bulk modulus. Inserting Equations 47 into Equations 46, we get

$$\rho_o V^2_{12} = \mu + \frac{1}{3K_o}\left[(3\lambda + 2\mu + \frac{3}{4}\lambda\alpha_6 + \frac{1}{2}\mu\alpha_6)\sigma_1 + (\frac{3}{4}\lambda\alpha_6 + \frac{1}{2}\mu\alpha_6)\sigma_2 + (\mu + \frac{1}{2}\mu\alpha_5 - \lambda - \frac{1}{2}\lambda\alpha_6)(\sigma_1+\sigma_2+\sigma_3)\right] \qquad (48)$$

$$\rho_o V^2_{13} = \mu + \frac{1}{3K_o}\left[(3\lambda + 2\mu + \frac{3}{4}\lambda\alpha_6 + \frac{1}{2}\mu\alpha_6)\sigma_1 + (\frac{3}{4}\lambda\alpha_6 + \frac{1}{2}\mu\alpha_6)\sigma_3 + (\mu + \frac{1}{2}\mu\alpha_5 - \lambda - \frac{1}{2}\lambda\alpha_6)(\sigma_1+\sigma_2+\sigma_3)\right]$$

The third order elastic constants α_5 and α_6 are related to Murnaghan's constants m and n by

$$\mu\alpha_5 = 2(\lambda - \mu + m - \frac{n}{2})$$
$$\mu\alpha_6 = 4\mu + n \qquad (49)$$

These relationships are obtained by comparing the strain energy function in Murnaghan's formulation and that of Truesdell.

If we insert Equations 49 into Equations 48, we get

$$\rho_o V^2_{12} = \mu + \frac{1}{3K_o}\left[(6\lambda + 4\mu + \frac{3}{4}\frac{\lambda n}{\mu} + \frac{1}{2}n)\sigma_1 + (3\lambda + 2\mu + \frac{3}{4}\frac{\lambda n}{\mu} + \frac{1}{2}n)\sigma_2 + (m - \frac{n}{2} - 2\lambda - \frac{1}{2}\frac{\lambda n}{\mu})(\sigma_1+\sigma_2+\sigma_3)\right]$$

$$\rho_o V^2_{13} = \mu + \frac{1}{3K_o}\left[(6\lambda + 4\mu + \frac{3}{4}\frac{\lambda n}{\mu} + \frac{1}{2}n)\,\sigma_1 + (3\lambda + 2\mu + \frac{3}{4}\frac{\lambda n}{\mu} + \frac{1}{2}n)\,\sigma_3 + (m - \frac{n}{2} - 2\lambda - \frac{1}{2}\frac{\lambda n}{\mu})\,(\sigma_1+\sigma_2+\sigma_3)\right] \quad (50)$$

For special stress fields, these equations become

$$\sigma_1 = \sigma_2 = \sigma_3 = -p_o$$
$$\rho_o V^2_{12} = \rho_o V^2_{13} = \mu - \frac{p_o}{3K_o}\left[3\lambda + 6\mu + 3m - \frac{n}{2}\right] \quad (51)$$

Uniaxial pressure in the 1-direction, i.e.,

$$\sigma_1 = -p_1\ ,\ \sigma_2 = \sigma_3 = 0$$
$$\rho_o V^2_{12} = \rho_o V^2_{13} = \mu - \frac{p_1}{3K_o}\left[4\lambda + 4\mu + m + \frac{1}{4}\frac{\lambda n}{\mu}\right] \quad (52)$$

Uniaxial pressure in the 2-direction,

$$\sigma_2 = -p_2$$
$$\rho_o V^2_{12} = \mu - \frac{p_2}{3K_o}\left[\lambda + 2\mu + m + \frac{\lambda}{4\mu}n\right]$$
$$\rho_o V^2_{13} = \mu - \frac{p_2}{3K_o}\left[m - 2\lambda - \frac{\mu+\lambda}{2\mu}n\right] \quad (53)$$

These relations (Equations 51 to 53) are identical with Equations 46 discussed in the previous section. The velocity of the Rayleigh waves can be obtained from Equation 43.

3.2 ULTRASONIC STRESS MEASURING DEVICE

The residual stress measuring device consists of an ultrasonic stress analyzer and a surface stress transducer. This ultrasonic stress measuring device is capable of measuring the transit time of ultrasonic waves with a resolution of better than one nanosecond or 10^{-9} seconds (Reference 45).

The transit times are measured by comparing two ultrasonic waveforms that are simultaneously generated at one millisecond intervals and nulled on the oscilloscope screen.

3.3 PROCEDURE TO DETERMINE THE RESIDUAL STRESSES

3.3.1 Principle of the Method

Measurement of the velocity of ultrasonic waves in metals has been used as a method for obtaining their elastic moduli. It is well known that application of a stress to the material will change the velocities of ultrasonic waves in the material, yielding a linear relationship between the applied stress and the change in velocity. This property of the material is attributed to the effect of higher order terms in the elastic moduli of the material, and has been treated in depth by a number of authors. The system utilized to perform residual stress measurements was designed to measure changes in ultrasonic velocity as a function of stress.

3.3.2 Surface Wave Technique

3.3.2.1 Determination of Surface Stresses

Surface waves propagate at the surface of the sample, and have characteristics of the longitudinal waves with particle motion parallel and perpendicular to the surface of the specimen. Figure 11(a) is a cross-section of a surface wave transducer showing the sending and receiving crystals coupled on a single piece of lucite. The crystals are x-cut quartz crystals mounted at the critical angle for surface wave propagation.

As an example, studies were conducted in Reference 38 on tensile specimens, stressed in uniaxial tension, within the elastic region, in an Instron test machine. Figure 11(b) is an oscilloscope trace of the reference pulse. The sweep time has been set so that a 10 μS duration sweep is produced, triggered at the time of the start of the variable delay. With the transducer attached to the sample, a received pulse is obtained. The

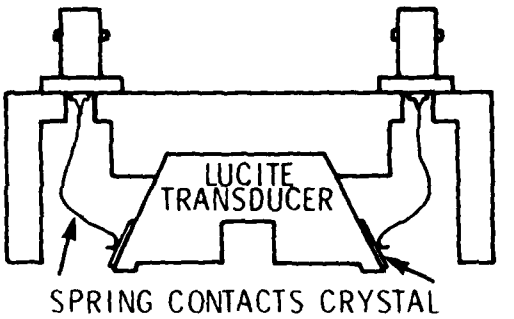

(a) A surface wave transducer

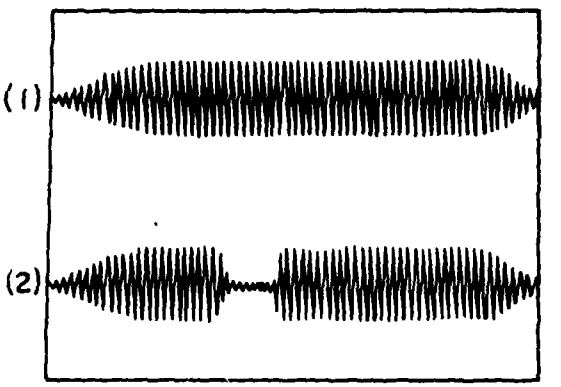

(b) Oscilloscope trace of the reference pulse in (1) has been nulled by the received pulse in (2)

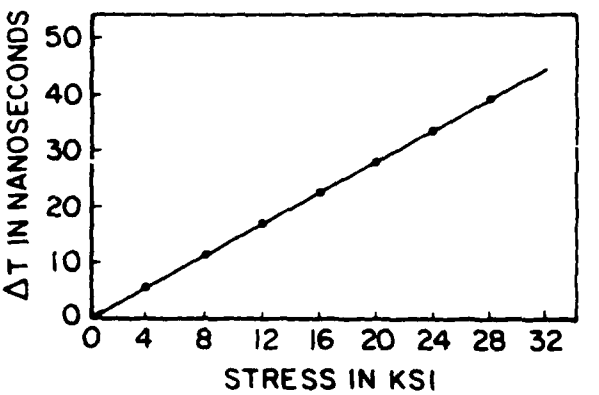

(c) Change in time of travel vs stress for surface waves for a 2014-T6 alloy stressed in tension

Fig. 11 Transducer, Reference and Received Pulses, and Calibration of a Rayleigh Surface Wave

reference pulse is made to coincide in time with the received pulse, so that added algebrically, a null is obtained (Figure 11(b)).

On application of a stress, the time of travel is changed, causing a shift in the received signal. The received pulse and the reference pulse are no longer in phase opposition and the wave form changes. The internal delay trigger is adjusted to obtain the null and the change in the time of travel determined. Measurements made on a 2014-T6 aluminum alloy show the variation of the changes in time of travel with applied stress in Figure 11(c). The linear behavior allows the definition of a constant, called the "stress acoustic constant." This constant has values which are different for tension and for compression,

$$\text{stress acoustic constant} = \frac{\Delta T}{\text{stress} \times \text{path length}} \qquad (54)$$

$$= \text{nanoseconds } (10^{-9} \text{ seconds}) \text{ per 1000 psi-inch}$$

The stress measured is the average stress to a depth of one wavelength below the surface of the specimen, since this corresponds to the depth of penetration of a surface wave. The study of the skin stresses is made possible by limiting the surface wave's depth of penetration just below the surface of the specimen. The velocity of the material is given by

$$V = \lambda_M f \qquad (55)$$

where λ_M is the wavelength and f is the frequency. For a constant velocity in a material, increasing the frequency of the ultrasonic wave will decrease the wavelength and so decrease the penetration of the wave. The study reported in Reference 38 was carried out at a frequency of 7 MHz which corresponds to a depth of 0.422 mm for a 2014-T6 aluminum alloy.

4.3.2.3 Determination of Residual Stresses

Residual stresses on the surface of a specimen may be measured in magnitude and direction using the

surface wave technique. The method uses a surface wave transducer mounted at a known orientation on the surface of the specimen in which the residual stresses are to be determined. The surface of the specimen is graduated at 10° intervals over its angular range of 360°. The surface wave transducer is placed on the surface of the specimen parallel to one direction on the specimen, and an ultrasonic surface wave is generated at one foot of the transducer, propagated through the sample, and received through the other foot. If the reference pulse is delayed by the transit time of the ultrasonic signal, then the two pulses, that is, the received signal and reference pulse, will add to each other. The vernier delay time control may be adjusted to place the two signals in phase opposition with each other. Further adjustment of the reference pulse amplitude will allow for a null to occur during the period when both signals are present. The transducer is then rotated through 10° and a second reading is obtained. Similar readings are made over the entire range of angles and these values are plotted on polar coordinates. Figure 12 shows the plot obtained in the analysis of 2014-T6 plate with residual surface stresses introduced by rolling. The principal axes of stress correspond to the maximum and minimum values of the time for propagation of the wave. For a sample that is completely stress free, a circular pattern is obtained, for the transit time is equal in all directions.

The following method is used to determine the magnitude and direction of residual or applied stresses on the surface of a specimen. A transducer coupled to the surface of a stress free sample is used to propagate a surface wave, and the transit time (t_{so}) is measured. The value obtained is for zero stress. Comparison of this value with the ones (t_s) measured on the surface of the specimen with residual (or applied) stress yield changes in transit time ($\Delta t = t_{so} - t_s$). The stress acoustic constant for the material may be used to calculate the surface stresses from the transit times of the ultrasonic wave in the stressed surface.

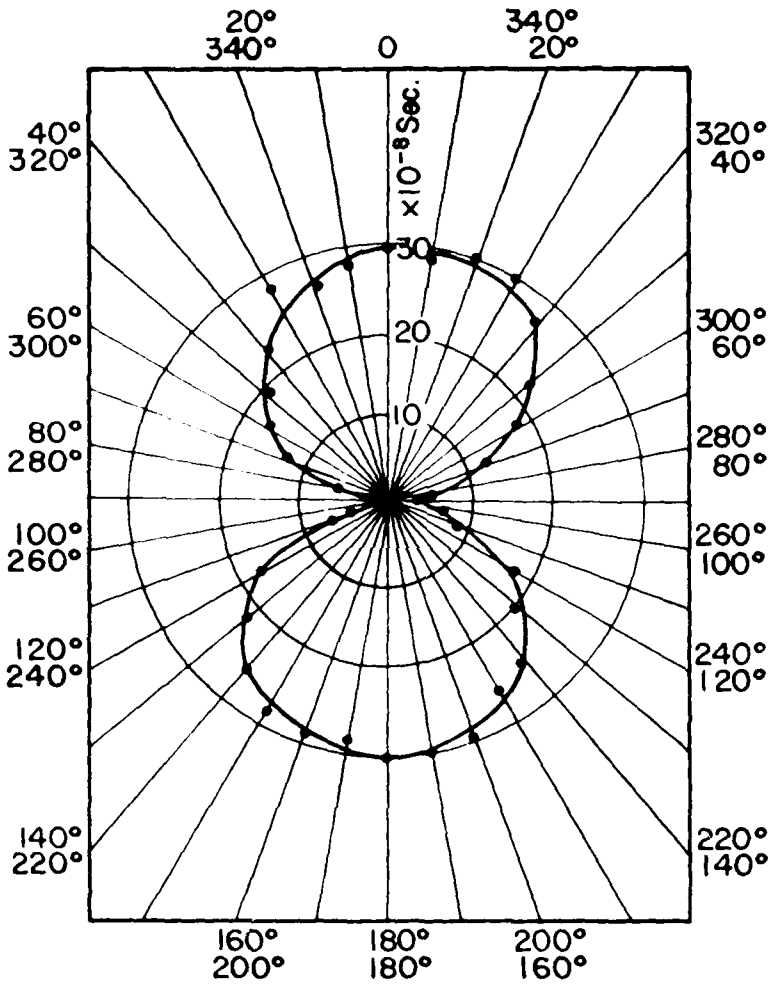

Figure 12. Change in Transit Time versus Transducer Orientation for Determining Surface Stress Directions.

3.3.2.3 Determination of Residual Stress Through the Thickness

As the name implies, a surface wave travels parallel to the surface penetrating the material to the depth of one wave length. A sample with residual stress may have isostress lines which lie in layers parallel to the surface of the sample. The sample containing residual stresses may be pictured as successive layers with different values of stresses joined together to constitute its thickness, and a plot of stress against the distance into the thickness of the sample will show a continuous curve. For the case of pure bending, the net stress through the sample will be zero, as there will be equal amounts of tension and compression in the sample. A surface wave traveling through the sample will penetrate to a layer one wavelength below the surface so that the stress measured by the wave will be an average to the depth of penetration, and thereby measure the average stress from the surface to any reasonable depth below the surface of the specimen. Hence, it is possible to determine the stress profile through the thickness of a specimen.

An experiment was performed (Reference 38) to determine the stress gradients in a sample stressed in bending. The loading apparatus is shown in Figure 13(a). This type of loading scheme introduces a constant bending moment in the sample within the region of the innermost supports. The induced stress varies linearly with distance from the neutral axis. The top surface of the sample is in tension, while the fibers of the sample below the neutral fiber are in compression. Surface waves were generated using a 1 MHz quartz crystal at frequencies of 1, 3, 5, and 7 MHz.

The average stress in a sample, when subjected to a constant bending moment, can be calculated (Figure 13(b)).

$$S_x = K_B x \tag{56}$$

$$S_{max} = Ka \; ; \quad S_x = S_{max} \cdot \frac{x}{a} \tag{57}$$

where K_B is a constant.

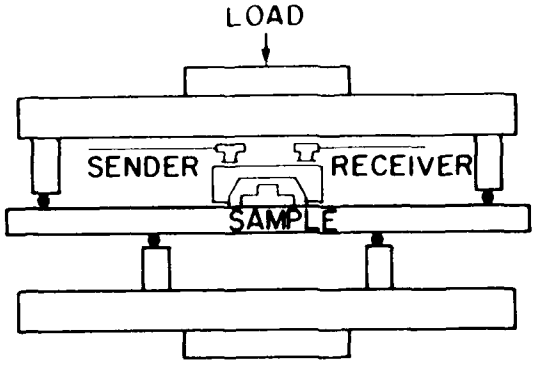

(a) Four-point loading device and surface wave transducer

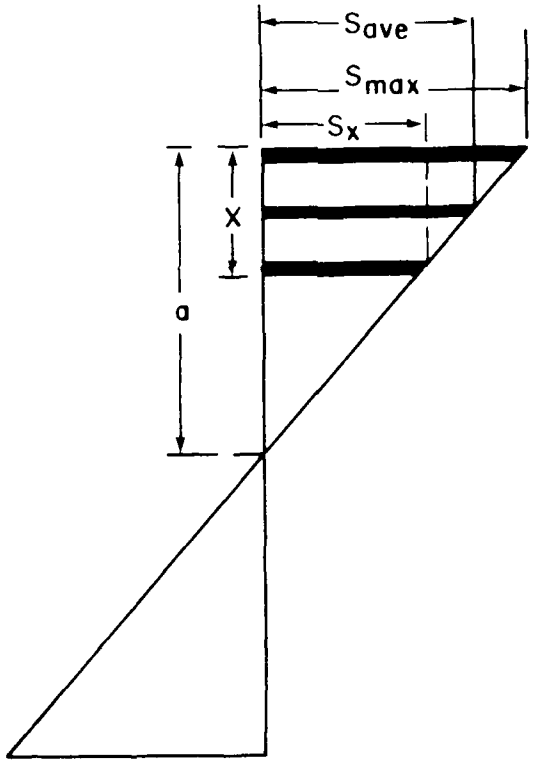

(b) Stresses through the thickness of a bending specimen

Figure 13. Four-Point Loading Device, Surface Wave Transducer, and Stresses Through the Thickness.

$$S_{average} = \frac{Sx + S_{max}}{2}$$

$$\frac{1}{2} S_{max} \left(1 + \frac{x}{a}\right) \qquad (58)$$

In an experiment, S_{max} can be determined as the average stress in the top layer of the specimen corresponding to the smallest wave length. By increasing the wavelength, the average stress corresponding to this increased wave length depth of penetration can be determined. From the stress equation (Equation 57), we can calculate S_x, the stress at the level x.

3.4 ULTRASONIC PROPERTIES OF POLYCARBONATE AND ACRYLIC PLASTIC MATERIAL

It may be necessary to experimentally determine the velocity of ultrasonic stress waves in polycarbonate and acrylic materials, as well as the second order and third order elastic constants for these materials by ultrasonic methods.

3.5 APPROXIMATE COST OF ULTRASONIC RESIDUAL STRESS MEASURING DEVICE

Stress analyzer complete system, including oscilloscope mainframe, three plug-in units, and a choice of two transducers.

Total cost (based on quotation dated August 1982) = $14,500.

SECTION 4

CONCLUSIONS AND RECOMMENDATIONS

The following conclusions and recommendations are based on [illegible] conducted during this review.

1. At present, the scattered-light photoelastic technique [illegible] used as a nondestructive method to study static, [illegible] thermal, and [illegible] elastoplastic problems of structural [illegible] employing plastics as the model material. The basic [illegible] features of the technique are well developed [illegible] tool. Very sophisticated and well developed experimental [illegible] are commercially available. However, the technique is at [illegible] a laboratory tool and needs the expertise of a [illegible] person to get reliable results. The method has [illegible] potential for development as a field experimental [illegible] tool.

2. At present, ultrasonic technique I based on Rayleigh [illegible] waves is widely used in measuring residual stresses in [illegible] steel and aluminum. The basic principles and the [illegible] of the technique are well developed and understood. [illegible] stress-velocity expressions in a stressed elastic [illegible] are available for longitudinal and shear waves. From [illegible], approximate expressions are derived for Rayleigh [illegible] waves. Further research is needed to directly develop [illegible] velocity expressions for Rayleigh surface waves [illegible] a stressed elastic medium. The experimental hard- [illegible] well developed, economical, simple to operate, and [illegible] used in field measurements. The application of this [illegible] to aircraft transparency plastic materials such as [illegible] and/or acrylics will have to be established. This may [illegible] determination of the velocities of ultrasonic Rayleigh [illegible] the second and third order elastic constants for such [illegible].

3. The ultrasonic technique II based on the energy reflec- [illegible] liquid-solid interface near the angle of incidence for

minimum reflection is at present used for evaluating certain characteristics and residual stresses in metals. The expressions for the energy ratios of reflected, refracted (longitudinal or shear) energies to incident energy is available. The transducers may be commercially available, but the goniometer needs to be designed and fabricated. This technique is reported to be very sensitive, but needs further development and research to make it a viable field measuring tool.

4. Magneto-photoelasticity is at present used to determine the states of stress in plastic bodies which do not show any optical effect by direct photoelastic observations, such as bending and residual stresses in plates. The basic equations and laboratory experimental hardware are available. This technique demands very sophisticated experimental hardware which is not commercially available. This is a very promising technique but still requires additional development before it could be recommended even as a laboratory experimental stress analysis tool.

5. Laser diffraction is, at present, used to characterize the distribution of crazes in plastics. The experimental hardware is very simple, relatively inexpensive, and available commercially. However, this technique needs additional development before it can be considered for characterizing the residual stresses in plastics. This is a very promising future experimental stress analysis tool which offers the potential for usage in the field.

It is recommended that: (1) ultrasonic technique I, based on Rayleigh surface waves, be evaluated for use on aircraft transparency plastic materials such as polycarbonates and acrylics and be further considered for development as a field tool to nondestructively determine the residual stresses in aircraft transparencies in their installed condition; (2) scattered-light techniques be demonstrated as a nondestructive technique for quantifying residual stresses in aircraft transparencies in the laboratory and that the experimental hardware required for field use be defined and, if practical, developed.

APPENDIX A

ULTRASONIC TECHNIQUE II (REFLECTION OF ULTRASONIC ENERGY AT A LIQUID-SOLID INTERFACE NEAR THE ANGLE OF INCIDENCE FOR MINIMUM REFLECTION)

The reflection of ultrasonic energy at a liquid-solid interface can often be used as a relatively rapid technique for evaluating certain material characteristics and the residual stresses, and under some conditions it is more sensitive than the standard ultrasonic methods. Nevertheless, boundary reflectivity has not been used extensively in material evaluation and residual stress measurement. In the following paragraphs a review of some long-known facts about ultrasonic reflectivity at liquid-solid boundaries are made and then "critical reflection" experiments and a goniometer are described (References 66 and 69).

A.1 BASIC PRINCIPLES AND THE EQUATIONS

Consider an ultrasonic beam incident upon a water-solid interface shown in Figure A.1(a). The geometrical relationships that exist between incident and refracted portions of the ultrasonic beam are generally described by Snell's law (Reference 69):

$$\frac{\text{Sin } \theta_i}{V_{L1}} = \frac{\text{Sin } \theta_\ell}{V_{L2}} = \frac{\text{Sin } \theta_s}{V_{S2}} \qquad \text{(A-1)}$$

where V_{L1} is the compressional wave velocity in water and V_{L2} and V_{S2} represent the longitudinal and shear wave velocities in the solid. When $V_{L2} > V_{S2} > V_{L1}$ the refraction angles are always larger than the angle of incidence and it is possible to produce critical refraction, i.e., the condition where the angle of refraction equals 90 degrees. When the angle of incidence is greater than that necessary to produce critical refraction of the shear wave, it may still be possible to excite surface waves along the boundary. Although the surface wave referred to here may differ slightly from the true Rayleigh wave (characterized by a

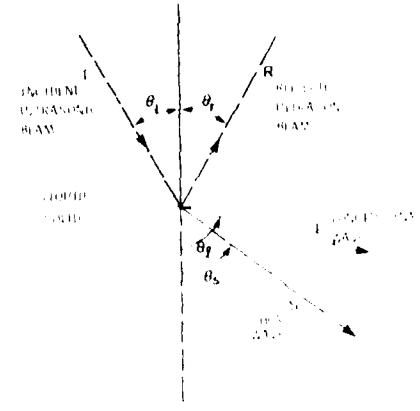

(a) Reflection and refraction at a liquid-solid interface

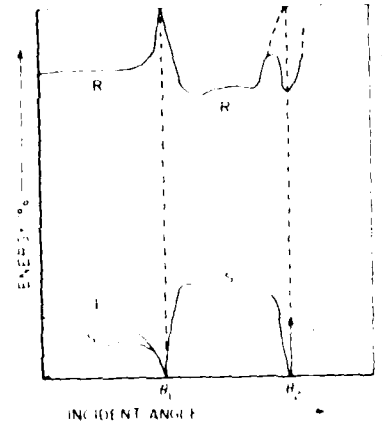

(b) Typical energy relationships at a liquid-solid interface

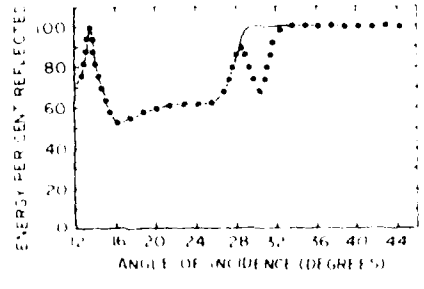

(c) Reflected energy versus angle of incidence for water-aluminum boundary showing calculated results (solid line) of Rayleigh and experimental results (open circles).

Figure A-1. Ultrasonic Energies at a Liquid-Solid Interface.

vacuum-solid boundary), the velocities are almost identical. There is one important difference between liquid-solid surface waves and vacuum-solid surface waves. At low megacycle frequencies, the latter may travel over long distances with relatively little attenuation. However, surface waves at a liquid-solid interface are rapidly attenuated due to radiation of compressional waves into the liquid. Snell's law can also be used to determine the angle of incidence for maximum excitation of surface waves. Since the "angle of refraction" is equal to 90 degrees, we get

$$\frac{\text{Sin } \theta_i}{V_{L1}} = \frac{1}{V_R} \qquad \text{(A-2)}$$

where V_R is the velocity of the surface wave. The exact value of V_R varies with the Poisson ratio for each solid, but is generally about $0.9\ V_{S2}$.

Consider next the partition of energy between the incident, reflected, and refracted portions of an ultrasonic beam. According to Mayers (Reference 67) and Ergin (Reference 68), the energy ratio of reflected to incident wave is given by

$$\left(\frac{R}{I}\right)^2 = \left\{ \frac{\text{Cos } \theta_r - A^* \text{Cos } \theta_i \ (1-B^*)}{\text{Cos } \theta_i + A^* \text{Cos } \theta_i \ (1-B^*)} \right\}^2 \qquad \text{(A-3)}$$

where

$$A^* = \frac{V_{L2}\ \rho_2}{V_{L1}\ \rho_1}$$

$$B^* = 2 \text{ Sin } \theta_S \text{ Sin } 2\theta_S \left[\text{Cos } \theta_S - \left(\frac{V_{S2}}{V_{L2}} \right) \text{Cos } \theta_S \right]$$

ρ_1 = density of liquid

ρ_2 = density of solid

The energy ratio of refracted longitudinal wave in the solid to the incident wave in the liquid is given by

$$\left(\frac{L}{I}\right)^2 = \left\{ \frac{2 \cos 2\theta_S \ (A^* \cos \theta_i \cos \theta_s)^{1/2}}{\cos \theta_i + A^* \cos \theta_i \ (1-B^*)} \right\}^2 \qquad (A-4)$$

The energy ratio of refracted shear wave to incident wave is then

$$\left(\frac{S}{I}\right)^2 = 1 - \left(\frac{R}{I}\right)^2 - \left(\frac{L}{I}\right)^2 \qquad (A-5)$$

Calculations of these ratios were made for a number of solids with the incident ray in water and oil.

Figure A.1(b) is taken from Reference 66 and illustrates the expected energy partition at a water-aluminum boundary when surface waves and attenuation are not considered. Under these conditions, the incident energy is partitioned only among the reflected wave (R) and refracted longitudinal (L) and shear (S) waves. At normal incidence, a refracted shear wave does not exist, so that the energy is partitioned between the reflected and the refracted longitudinal wave. The exact division at normal incidence is dependent on the impedance mismatch at the boundary, and the amplitude ratio of the reflected and incident waves is given by

$$\frac{A_R}{A_i} = \frac{\rho_2 V_{L2} - \rho_1 V_{L1}}{\rho_2 V_{L2} - \rho_1 V_{L1}} \qquad (A-6)$$

where $\rho_1 V_{L1}$ and $\rho_2 V_{L2}$ are the characteristic impedances of the water and solid, respectively. As the angle of incidence is increased, some energy goes into the refracted shear wave until the critical angle for the refracted longitudinal wave is approached. At this critical angle, θ_1, all the energy is theoretically reflected back into the water. At higher angles, the refracted shear wave (S) receives a fairly large percent of the incident energy until it also approaches its critical angle, θ_2. In this somewhat simplified picture, the incident energy would be totally reflected at all higher angles. When the possibility of surface waves is admitted to the theory, a more

complex situation exists and a major change in reflection effects occur at an angle of incidence near to that which produces critical refraction of the shear wave. A comparison of theoretical and experimental reflection data is given in Figure A.1(c). The reflected energy is plotted as a function of angle of incidence for a water-aluminum interface at an ultrasonic frequency of 5 megacycles per second. The solid curve is repeated from Figure A.1(b) and represents the theoretical reflection variations when surface waves and attenuation are not considered. The open circles represent experimental data. The agreement is very good except at angles of incidence near 31 degrees. The first maximum at 14 degrees is related to critical refraction of the longitudinal wave. The experimentally observed minimum in reflected signal at $_{\text{minimum}}$ of 31 degrees is related to the excitation of surface waves. It is this minimum that is most sensitive to physical properties of the solid.

A.2 PRINCIPLES OF A GONIOMETER

In order to ensure that the equality of the angles of incidence and reflection is maintained in the water and that the directions of these beams intersect at the same point, it is necessary to provide for certain mechanical features. In Figure A.2, a circular roller is shown which is moved up and down a vertical axis, increasing or decreasing the angle between the goniometer arms on either side. The pivot point P is in the surface or slightly below it for maximum intensity because of a small beam displacement on reflection. If the two arms are separated at a fixed distance "$\bar{a}$" from a pivot A, while the radius of the roller is "b" with center at "B", the condition that P shall be fixed requires that the heights of the two points A and B should be maintained in the same ratio as a/b, that is, h_1 and h_2 in the diagram are given by $h_1/h_2 = \bar{a}/\bar{b}$. Consequently, a vertical screw in the line of DBAP must move B up or down faster than A but in this ratio.

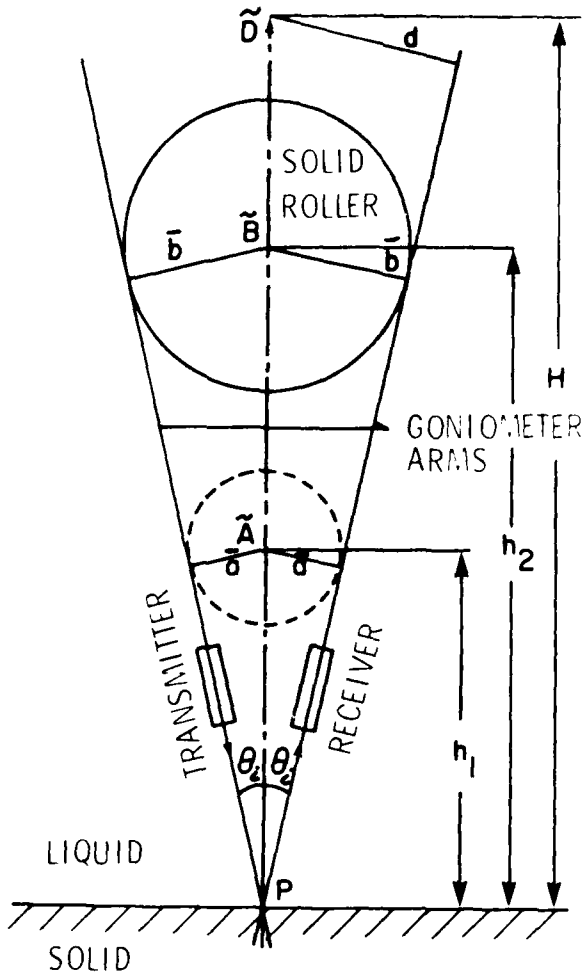

(a) Geometrical principles of transportable goniometer

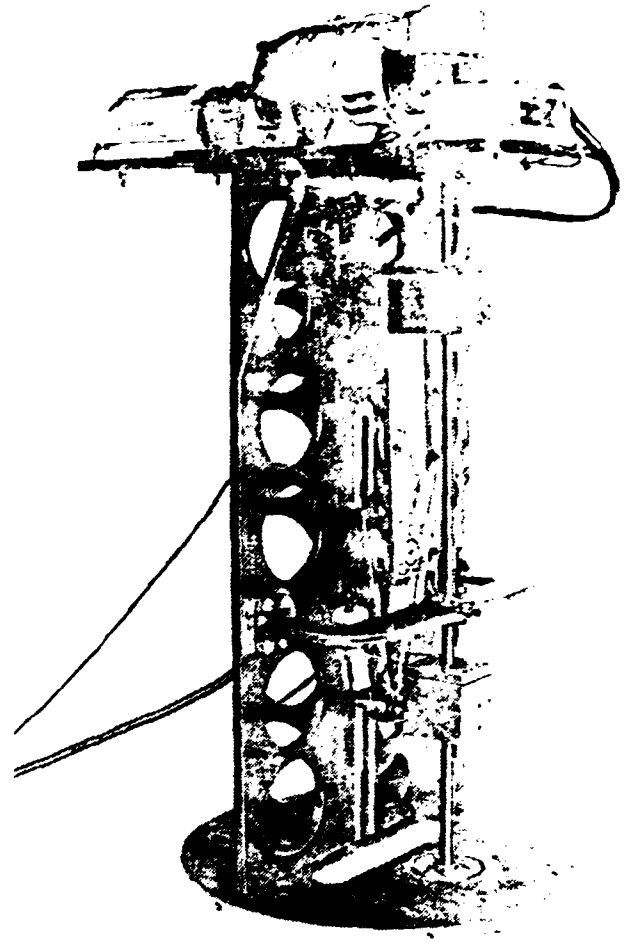

(b) Goniometer

Figure A-2. Elements of Ultrasonic Goniometer.

The instrument is shown in Figure A.2. The instrument is held together in a rigid framework comprising a circular base plate onto which is welded a vertical main plate and perpendicular to it at the rear, two strengthening members. They support the top platform on which there is mounted a motor drive and gear box to operate the vertical lead screw. There is also a revolution counter which records the angular rotation of the screw and the reading of this counter can easily be calibrated as a function of the angle of incidence θ_i in Figure A.2(a).

The lead screw has two sections separated by a bearing and supporting frame which is screwed to the main body. The upper part of the screw has twice the pitch of the lower part, and the rotation is transmitted from the screw into the vertical movements of the roller and the pivot, respectively. The bearings of the roller and the pivot are held in position by milled slots in the main vertical plate. The geometry of the system requires that the two ultrasonic probes acting as transmitter and receiver must have their axes along the lines of the tangents to the two circles. In the instrument shown, they are clamped onto the side of two metal arms held onto the roller by springs. The actual choice of positions for points A and B is therefore adjusted in order to ensure that the geometrical condition is fulfilled. The transducers used were in the frequency range of 1 to 10 MHz and had diameters between 5 and 15 mm.

In operation the instrument must be immersed in water or other liquid sufficient to cover the lower ends of the transducer and receiver. Thus, the lower part of the instrument has to be protected against corrosion and it is advisable for the liquid to contain a suitable inhibitor. The water tank can be replaced by the use of a flexible bag of polythene which can adapt to the surface shape. This will introduce a thin layer of material between the liquid and solid interface, but the effect on any measurements should be negligible in most practical cases.

A.2.1 Calibration of the Goniometer

The first element of calibration required is to establish the relationship between the revolutions of the lead screw and the angle θ. The second calibration required is to establish the variation of some angle θ, either a critical reflection angle or the peak of the Rayleigh wave intensity as a function of applied stress or strain. This condition, established under known conditions, is then available for the determination of unknown residual stress or strain. In the course of this calibration, the load was fixed and the angular position scanned over a range of one degree or more in order to find the minimum of reflected energy corresponding to the maximum Rayleigh wave intensity. The actual strain in the specimen surface was determined by reference to electrical resistance gages suitably attached. Figure A.3(a) shows the calibration obtained from a steel. Measurable changes could occur due to temperature variations in the water or oil bath. Consequently, the extent of this variation is to be established, and in subsequent measurements the temperature is to be determined and a correction applied when necessary.

A.2.2 Applications of Goniometer

A very successful metallurgical application of the goniometer was achieved in the study of the effects of composition variables and case hardening treatments on the residual stress in steels for gear blanks. Figures A.4(a) and A.4(b) illustrate the primary measurements on the instrument for radial and circumferential directions at the mid-radial positions on the flat faces of the blanks. It is reported that x-ray methods give indications of surface stress to a depth in the region of 25 μm. The ultrasonic method is less superficial in that the penetration is of the order of 250 μm.

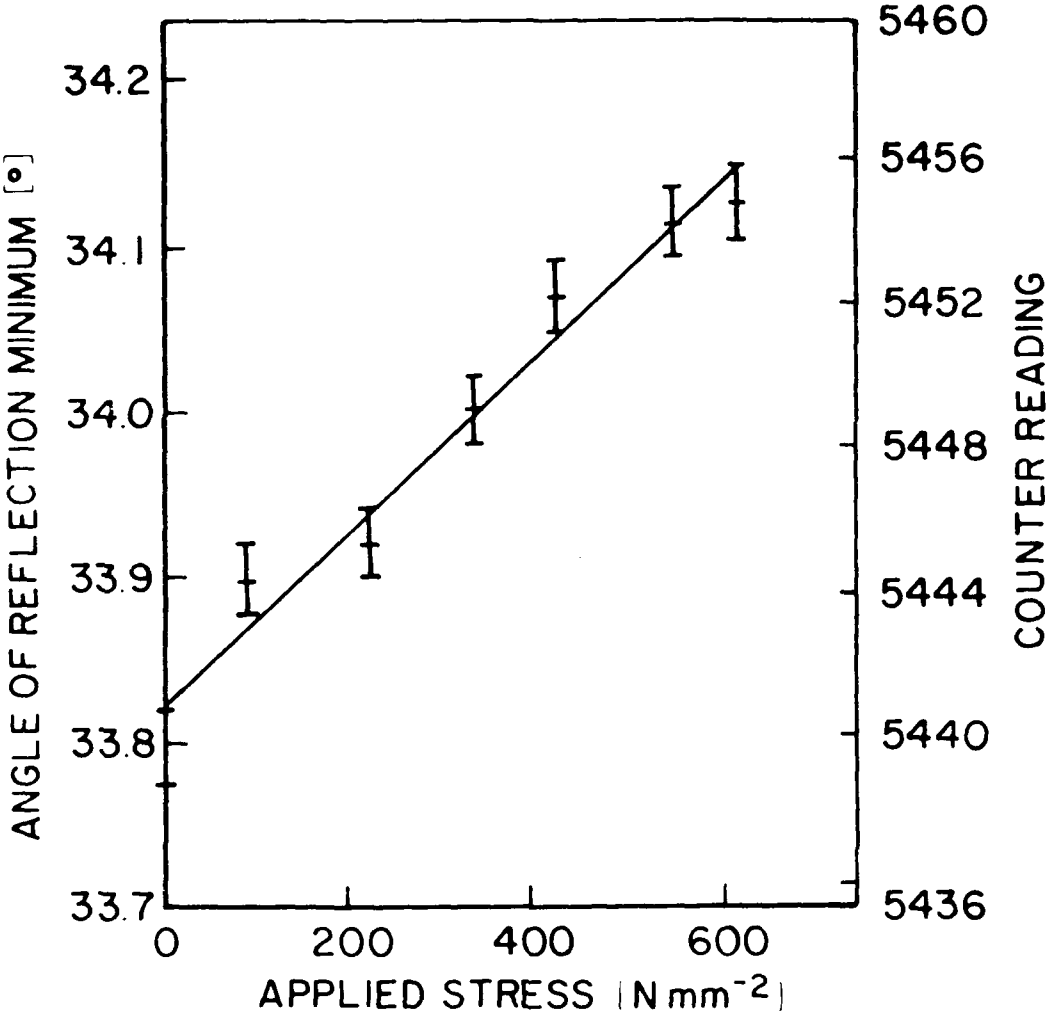

(a) Variation of the angle of reflection minimum with applied stress

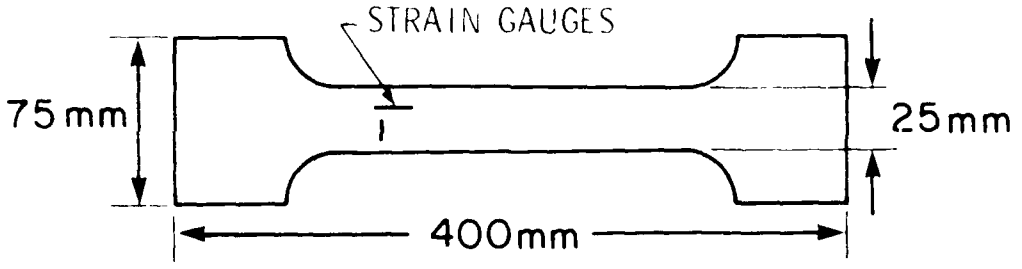

(b) Strain gauge network and specimen

Figure A-3. Calibration of Goniometer.

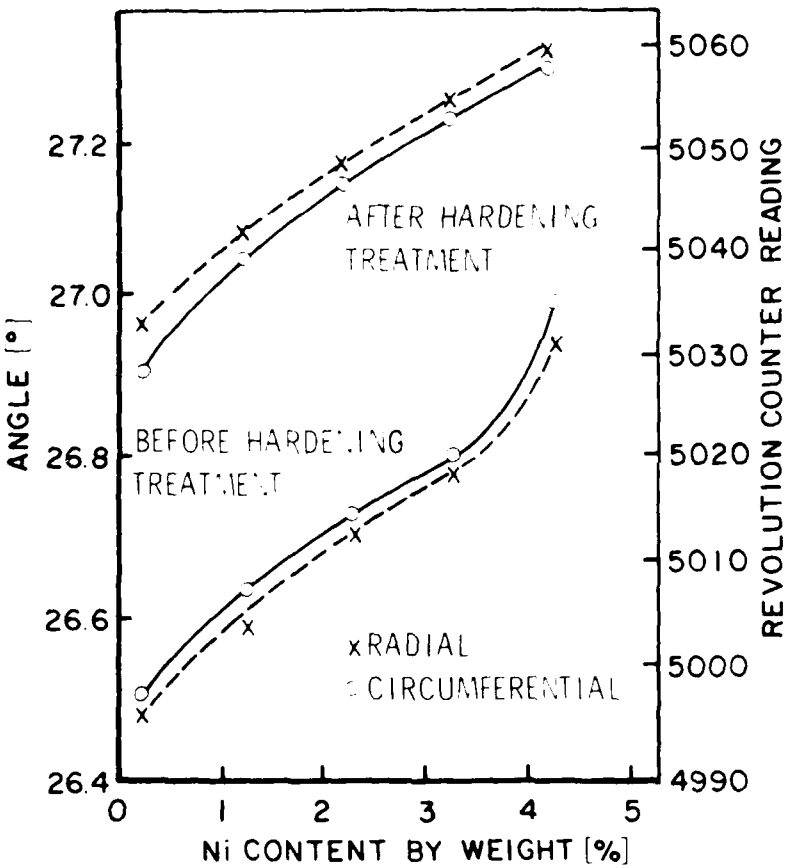

(a) Variation of reflection minima with nickel content

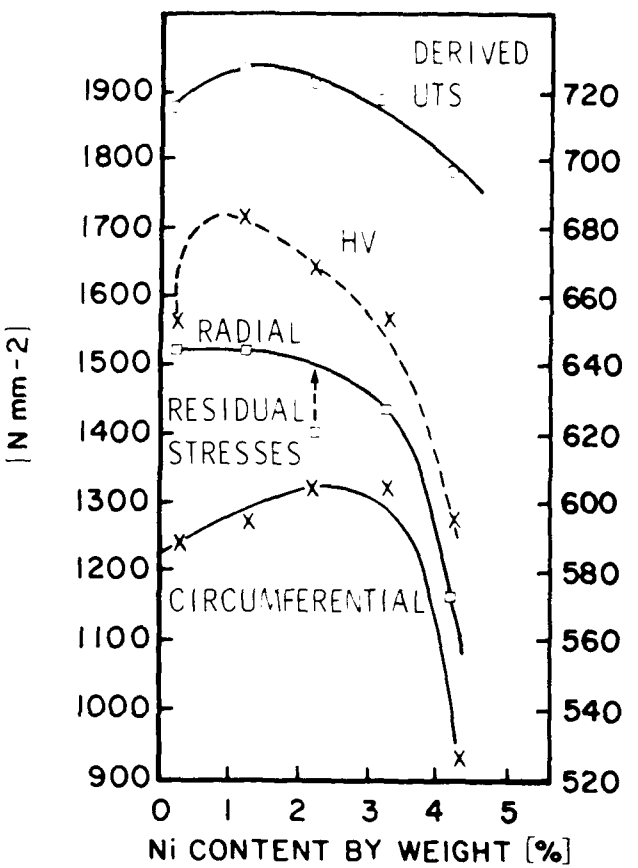

(b) Variation of surface hardness and stresses

Figure A-4. Variation of Residual Stress and Hardness with Nickel in Steel.

REFERENCES

1. MIL-HDBK-17A, Plastics for Aerospace Vehicles, Part II Transparent Glazing Materials, June 1977, pp. 3-3 to 3-4, II-28 to II-35.

2. Russel, E. W., Studies on Polymethyl Methacrylate, Part III. Crazing Effects, R.A.E. Report No. Chem. 447, August 1948.

3. Russel, E. W., "Crazing of Cast Polymethyl Methacrylate," Nature (London) 165, No. 4186, 91, January 1950

4. Bauer, J. A., J. Marin and C. C. Hsio, "Creep and Damping Properties of Polystyrene," Journal of Applied Physics, Vol. 20, June 1949, pp. 507-517.

5. Weller, R., "Three-Dimensional Photoelasticity Using Scattered Light," Journal of Applied Physics, Vol. 12, August 1941, pp. 610-616.

6. Weller, R. and J. K. Bussey, Photoelastic Analysis of Three-Dimensional Stress Systems Using Scattered Light, NACA Technical Note No. 737, November 1939.

7. Jessop, H. T., "The Scattered Light Method of Exploration of Stresses in Two- and Three-Dimensional Models," British Journal of Applied Physics, Vol. 2(9), September 1951, pp. 249-260.

8. Frocht, M. M. and L. S. Srinath, "A Non-Destructive Method for Three-Dimensional Photoelasticity," Proceedings of the Third U. S. National Congress of Applied Mechanics, A.S.M.E., 1958, pp. 329-336.

9. Srinath, L. S. and M. M. Frocht, "Scattered-Light in Photoelasticity - Basic Equipment and Techniques," Proceedings of the Fourth U. S. National Congress of Applied Mechanics, A.S.M.E., 1962, pp. 775-781.

10. Srinath, L. S., "Analysis of Scattered-Light Methods in Photoelasticity," Experimental Mechanics, Vol. 26, No. 2, October 1969, pp. 463-468.

11. Srinath, L. S. and A.V.S.S.R.Sarma, "Determination of the Optically Equivalent Model in Three-dimensional Photoelasticity," Experimental Mechanics, Vol. 31, No. 1, March 1974, pp. 118-122.

12. Cheng, Y. F., "Some New Techniques for Scattered-Light Photoelasticity," Experimental Mechanics, Vol. 20, No. 2, November 1963, pp. 275-278.

13. Cheng, Y. F., "A Dual Observation Method for Determining Photoelastic Parameters in Scattered-Light," Experimental Mechanics, Vol. 7, No. 3, March 1967, pp. 140-144.

14. Cheng, Y. F., "An Automatic System for Scattered-Light Photoelasticity," Experimental Mechanics, Vol. 26, No. 2, September 1969, pp. 407-412.

15. Cheng, Y. F., "A Scattered Light Photoelastic Method for the Determination of Tempered Stresses in Aircraft Windshields," Strain, Vol. 3, No. 2, 1967, pp. 17-22.

16. Bateson, S., J. W. Hunt, D. A. Dalby, and N. K. Sinha, "Stress Measurement in Tempered Glass Plates by Scattered Light Method with a Laser Source," Ceramic Bulletin, Vol. 45, No. 2, February 1966, pp. 193-198.

17. Swinson, W. F., J. L. Turner, and W. F. Ranson, "Designing with Scattered-Light Photoelasticity," Experimental Mechanics, Vol. 37, No. 2, November 1980, pp. 397-402.

18. Davis, J. B. and W. F. Swinson, "Experimental Investigation of Transient Thermal Stresses in a Solid Sphere," Experimental Mechanics, Vol. 8, No. 9, September 1968, pp. 404-408.

19. Braswell, D. W., W. F. Ranson, and W. F. Swinson, "Scattered-Light Photoelastic Thermal Stress Analysis of a Solid-Propellant Rocket Motor," Journal of Spacecraft, Vol. 5, No. 12, December 1968, pp. 1411-1416.

20. Aderholt, R. W., W. F. Ranson, and W. F. Swinson, "Scattered-Light Photoelastic Stress Analysis of a Solid-Propellant Rocket Motor," Experimental Mechanics, Vol. 27, No. 2, November 1970, pp. 481-485.

. [illegible], S. E., C. E. Taylor, and I. M. Daniel, "A [illegible] Ruby-Laser System for Dynamic Photomechanics: [illegible] to Transmitted- and Scattered-Light Photo-[illegible]," Experimental Mechanics, Vol. 26, No. 2, [illegible] 1969, pp. 385-393.

. [illegible], J. [illegible], E. W. Aderholdt, W. F. Ranson, and [illegible], "Scattered-Light Rosette," Experimental [illegible], Vol. [illegible] December 1971, pp. 554-559.

. [illegible], W. [illegible] and C. E. Bowman, "Application of Scattered [illegible] Photoelasticity to Doubly Connected Tapered Torsion [illegible]," Experimental Mechanics, Vol. [illegible] June 1966, [illegible]. 297-305.

. [illegible], W. W., J. M. McKinney, W. F. Ranson, and W. T. Swanson, "Effect of Rotating Secondary Principal [illegible] Scattered-Light Photoelasticity," Experimental Mechanics, Vol. 10(4), April 1970.

. [illegible], J. E. and H. Pih, "Three-Dimensional Scattered-Light Stress Analysis of Discontinuous Fiber-reinforced Composites," Experimental Mechanics, Vol. 30, No. 2, [illegible] 1973, pp. 294-298.

. Homann, J. H. and R. J. Becherer, "A Study of the Scattered-Light Technique in Two-Dimensional Problems," Experimental Mechanics, Vol. 29, No. 1, January 1972, pp. 43-46.

27. Johnson, E. L., The Measurement of Elastic-Plastic Stresses by Photomechanics, Ph.D. Thesis submitted to the University of Pittsburgh, 1973.

28. Johnson, E. L., "Measurement of Elastic-Plastic Stresses by Scattered-Light Photomechanics," Experimental Mechanics, Vol. 33, No. 1, June 1976, pp. 201-208.

. [illegible]-Peterson, J. P., "A Scattered-Light Method in Photoelasticity," Experimental Mechanics, Vol. 31, No. 2, August 1974, pp. 317-322.

30. Cernosek, J., "On the Effect of Rotating Secondary Principal Stresses in Scattered-Light Photoelasticity," Experimental Mechanics, Vol. 30, No. 2, July 1973, pp. 273-279.

31. Robert, A. J., "New Methods in Photoelasticity," Experimental Mechanics, Vol. 24, No. 1, May 1967, pp. 224-232.

32. Robert, A. and Guillemet, "New Scattered Light Method in Three-Dimensional Photoelasticity," British Journal of Applied Physics, Vol. 5, 1964, pp. 567-578.

33. Drucker, Daniel C. and R. D. Mindlin, "Stress Analysis by Three-Dimensional Photoelastic Methods," Journal of Applied Physics, Vol. 11, November 1940, pp. 724-732.

34. Berghaus, D. G., "Simplifications for Scattered-Light Photoelasticity when using the Unpolarized Incident Beam,: Experimental Mechanics, Vol. 21, No. 10, October 1981, pp. 394-400.

35. Heman, J. H. and R. J. Becherer, "Stresses and Strains in Axisymmetric Problems Using Scattered-Light Photoelasticity," Experimental Mechanics, Vol. 29, No. 1, June 1977, pp. 233-236.

36. Bulletin T-408, Scattered-Light Photoelasticity, Photolastic Division, Measurements Group, Inc., 1981.

37. Bulletin S-119, 301 Series Scattered-Light Polariscope, Photolastic Division, Measurements Group, 1981.

38. Noronha, P. J., J. R. Chapman, and J. J. Wert, "Residual Stress Measurement and Analysis Using Ultrasonic Techniques," Journal of Testing and Evaluation, JTEVA, Vol. 1, No. 3, May 1973, pp. 209-214.

39. Noronha, P. J. and J. J. Wert, "An Ultrasonic Technique for the Measurement of Residual Stress," Journal of Testing and Evaluation, JTEVA, Vol. 3, No. 2, March 1975, pp. 147-152.

40. Martin, B. G., "The Measurement of Surface and Near-Surface Stress in Aluminum Alloys Using Ultrasonic Rayleigh Waves," Material Evaluation, Vol. 32, November 1974, pp. 229-234.

41. Martin, B. G., "Rayleigh-Wave Velocity Stress and Preferred Grain Orientation in Aluminum," Non-Destructive Testing, August 1974, pp. 199-203.

42. Gordon, Jr., B. E., and T. O. P. Speidel, "Stress Measurement by Ultrasonic Techniques," SESA Fall Meeting, October 1973, p. 1-30.

43. Adler, L., K. V. Cook, B. R. Dewey, and R. T. King, "The Relationship Between Ultrasonic Rayleigh Waves and Surface Residual Stress," Materials Evaluation, July 1973, pp. 93-96.

44. McKannan, E. C., "Ultrasonic Measurement of Stress in Aluminum," Non-destructive Testing: Trends, Techniques, Proceedings of the Second Technology Status and Trends Symposium, NASA SP-5082, 1967, pp. 43-54.

45. , Ultrasonic Stress Analyser, Ultrasonic Analysis, Inc., Stamford, CT.

46. Brillouin, L., "Les Lois De L'Elasticité Sous Forme Tensorielle Valable Pour des Coordonnes Quelconques," Annalues De Physique, Vol. 3, 1925, pp. 251-298.

47. Murnaghan, F. D., "Finite Deformations of an Elastic Solid," American Journal of Mathematics, Vol. 59, 1937, pp. 235-260.

48. Murnaghan, F. D., Finite Deformation of an Elastic Solid, John Wiley & Sons, Inc., New York, 1951.

49. Hughes, D. S., and J. L. Kelly, "Second-order Elastic Deformation of Solids," Physical Review, Vol. 92, No. 5, December 1, 1953.

50. Cook, E. G. and H. E. Van Valkenburg, "Surface Waves at Ultrasonic Frequencies," ASTM Bulletin, May 1954, pp. 81-84.

51. Lockett, F. J., "Effect of Thermal Properties of a Solid on the Velocity of Rayleigh Waves," Journal of Mechanics and Physics of Solids, Vol. 7, 1958, pp. 71-75.

52. McSkimin, H. J., "Notes and References for the Measurement of Elastic Moduli by Means of Ultrasonic Waves," Journal of the Acoustical Society of America, Vol. 33, No. 5, May 1961, pp. 606-615.

53. Bateman, T., W. P. Mason, and H. J. McSkimin, "Third-Order Elastic Moduli of Germanium," Journal of Applied Physics, Vol. 32, No. 5, May 1961, pp. 928-936.

54. Toupin, R. A. and B. Bernstein, "Sound Waves in Deformed Perfectly Elastic Materials. Acoustoelastic Effect," The Journal of the Acoustical Society of America, Vol. 33, No. 2, February 1961, pp. 216-225.

55. Bradfield, G., "The Influence of Texture and Plastic Deformation on the Elasticity of Polycrystalline Metals," Fourth International Congress on Acoustics, Copenhagen, August 1962.

56. Bradfield, G., Use in Industry of Elasticity Measurements in Metals with the Help of Mechanical Vibrations, Notes on Applied Science No. 30, National Physical Laboratory, London, 1964.

57. Thurston, R. N. and K. Brugger, "Third-Order Elastic Constants and the Velocity of Small Amplitude Elastic Waves in Homogenously Stressed Media," Physical Review, Vol. 133, No. 6A, March 1964.

58. Thurston, R. N., "Effective Elastic Coefficients for Wave Propagation in Crystals Under Stress," Journal of the Acoustical Society of America, Vol. 37, No. 2, February 1965, pp. 348-356.

59. Smith, R. T., R. Stern, and W. B. Stephens, "Third-Order Elastic Moduli of Polycrystalline Metals from Ultrasonic Velocity Measurements," Journal of the Acoustical Society of America, Vol. 40, No. 5, 1966, pp. 1002-1008.

60. Viktorov, I. A., Rayleigh and Lamb Waves, Plenum Press, New York, 1967.

61. Tokuoka, T. and M. Saito, "Elastic Wave Propagations and Acoustical Birefringence in Stressed Crystals," Journal of the Acoustical Society of America, Vol. 45, No. 5, 1969, pp. 1241-1246.

62. Lambert, M. A., "Détermination non Destructive des Profondeurs de Cémentation," Congres Mesucora, 1973, pp. 1-10.

63. Bach, F. and V. Askegaard, "General Stress-Velocity Expressions in Acoustoelasticity," Experimental Mechanics, 1978, pp. 69-75.

64. Okada, K., "Stress-acoustic Relations for Stress Measurement by Ultrasonic Technique," Journal of Acoustical Society of Japan, Vol. 1, No. 3, 1980, pp. 193-200.

65. Tokuoka, T. and Y. Iwashimizu, "Acoustical Birefringence of Ultrasonic Waves in Deformed Isotropic Elastic Materials," International Journal of Solids and Structures, Vol. 4, 1968, pp. 383-389.

66. Andrews, K. W. and R. L. Keightley, "An Ultrasonic Goniometer for Surface Stress Measurement," Ultrasonics, September 1978, pp. 205-209.

67. Mayer, W. G., "Reflection and Refraction of Mechanical Waves at Solid-Liquid Boundaries," Journal of Applied Physics, Vol. 34, No. 4 (Part 1), April 1973, pp. 909-911.

68. Erqin, K., "Energy Ratio of the Seismic Waves Reflected and Refracted at a Rock-Water Boundary," Bulletin of Seismic Society of America, Vol. 42, 1952, pp. 349-372.

69. Rollins, Jr. F. R., "Critical Ultrasonic Reflectivity--A Neglected Tool for Material Evaluation," Materials Evaluation, Vol. 24, 1966, pp. 683-689.

70. Rollins, Jr., F. R., "Ultrasonic Reflectivity at a Liquid-Solid Interface Near the Angle of Incidence for Total Reflection," Applied Physics Letters, Vol. 7, No. 8, October 1965, pp. 212-216.

71. Bradfield, G., "The Ultrasonic Goniometer and its Applications," Non-destructive Testing, Vol. 2, February 1968, pp. 165-172.

72. Weinstein, M. S., "On the Failure of Plane Wave Theory to Predict the Reflection of a Narrow Ultrasonic Beam," Journal of the Acoustical Society of America, Vol. 24, No. 3, May 1952, pp. 284-287.

73. Aben, H. K., "Principles of Magneto-Photoelasticity," Experimental Stress Analysis, Institution of Mechanical Engineers, 1970.

74. Hsiao, C. C. and A. Cers, "Laser Diffraction of Crazed Polymers," American Society of Chemical Society, Vol. 34, No. 2, 1974, pp. 223-228.